Korean J. Chem. Eng., 37(11), 1836-1858 (2020)
DOI: 10.1007/s11814-020-0625-z

pISSN: 0256-1115
eISSN: 1975-7220

Effect of Biot number on unsteady reaction-diffusion phenomena and analytical solutions of coupled governing equations in porous particles with various shapes

Young-Sang Cho† and Sohyeon Sung

Department of Chemical Engineering and Biotechnology, Korea Polytechnic University,
237 Sangdaehak-ro, Siheung-si, Gyeonggi-do 15073, Korea
(*Received 20 February 2020 • Revised 3 June 2020 • Accepted 7 July 2020*)

Abstract−Analytical solutions of transient concentration profile inside particles were calculated by solving rection-diffusion equation in spherical, cylindrical, and slab-type porous particles, assuming first order irreversible reaction. Time-dependent concentration in bulk fluid phase was assumed as exponential decay for each particle, and convective boundary conditions were taken using arbitrary Biot number to obtain a general solution by eigenfunction expansion or Laplace transform method. Factors affecting average transient concentration inside particles were studied by adjusting Biot number, reaction time, and Thiele modulus as well as the position inside particles. To predict transient bulk concentration in batch photocatalytic reactor containing porous particles, coupled differential equations were solved by Laplace transform to obtain analytical solutions of bulk concentration as well as average concentration inside porous particles as a function of reaction time. The factors affecting transient concentrations were investigated by adjusting the concentration and porosity of the catalytic particles, morphology of the particles, and Thiele modulus in batch-mode reactor to study reduction speed of reactant concentration during photocatalytic reaction. The solutions from coupled differential equations were useful for the prediction of transient behavior in batch-type photocatalytic reactor and were compared with the results from CSTR containing slab-type photocatalytic particles with various space time.

Keywords: Porous Particles, Reaction-diffusion Equation, Eigenfunction Expansion, Biot Number, Time-dependent Boundary Condition, Coupled Differential Equations, Laplace Transform

INTRODUCTION

Over several decades, porous materials have been intensively studied for various industrial applications, such as membrane separation, filters, construction materials for sound absorbing or insulating structures, and adsorbent materials in purification of gas stream or wastewater [1-6]. In addition, catalytic supports or photocatalytic materials have been fabricated as particulate form in packed bed or slurry-type reactors in powder technology [7,8]. Recently, porous photocatalytic materials have been also applied for generation of hydrogen energy in water-splitting systems [9]. Besides synthesis and applications, modeling of transient behavior of reactant inside or outside of these porous particles is also important to understand the physicochemical background in related areas of chemical engineering, since mathematical analysis on the porous materials during reaction is vital to effective operation of reaction equipment.

Since the measurement of reactant concentration inside porous particles is impossible by experimental technique, prediction of such values by numerical scheme or mathematical analyses can provide engineering insights for mass transport or reaction behavior. Additionally, calculation of bulk concentration is also crucial for design of reactors containing porous catalytic particles, since determination of adjustable parameters can be considered as design factors. Although numerical simulation is a powerful means for these research topics, mathematical analyses are still challenging for treatment of reaction-diffusion equation subject to arbitrary boundary conditions on a particle surface to get approximate or exact solutions by inverse Laplace transform including our previous results [10-12]. Unlike conventional reaction-diffusion equation, generation of chemical species by first-order reaction has been also studied by eigenfunction expansion method, which is useful degradation behavior of PLGA particles [13]. Unlike mathematical analyses on conventional porous particles, porous spherical particles with inert cores have been also treated for reaction-diffusion phenomena in batch or packed bed reactor by Laplace transform [14]. However, further researches are still necessary, since previous studies on analytical or approximate solutions were not performed by considering the effect of Biot number, which is important to estimate mass transfer resistance between bulk phase and inner region of porous particles with various morphologies. The mathematical treatment of coupled differential equations on transient behavior of bulk and particle phase can be also considered to predict the analytical solutions for more precise prediction in slurry-type batch or CSTR reactors.

In our previous research, the concentration profile and average dimensionless concentration inside catalytic particles in various coordinate systems were obtained analytically by solving reaction-diffusion equation assuming infinite value of Biot number subject to various time-dependent boundary conditions [15]. In the present article, more general solutions were obtained for arbitrary valued Biot numbers by eigenfunction expansion method to establish

†To whom correspondence should be addressed.
E-mail: yscho78@kpu.ac.kr, yscho78@gmail.com

transient concentration profiles inside catalytic particles in spherical, cylindrical, and rectangular coordinates for reaction-diffusion equation with first-order irreversible reaction. Additionally, the transient bulk concentration of methylene blue was measured experimentally using macroporous titania fibers as cylindrical particles, to compare with the predicted concentration inside particles from mathematical solution. In this study, time-dependent boundary condition was restricted to exponentially decaying bulk concentration, which is suitable for catalytic reactions or adsorption in slurry-type reactors [15]. To predict transient bulk concentration and average concentration inside particles simultaneously, coupled partial differential equations in spherical, cylindrical, and slab-type porous photocatalytic particles were also solved by Laplace transform method to obtain approximate or exact solutions of reaction-diffusion equation for any value of particle concentration as adjustable parameter. In this study, the effects of various parameters such as reaction time, Thiele modulus, and position inside catalytic particles on transient concentrations were studied to predict the behavior of batch-type slurry reactor, which is necessary for various environmental treatments as in the dye industry. For comparison, continuous operation of photocatalytic reactor was also treated briefly to study the effect of space time in CSTR reactor containing slab-type photocatalytic particles.

MATERIALS AND METHODS

1. Synthesis of Macroporous Titania Fibers by Electro-spinning

Colloidal templating method was adopted to prepare macroporous titania fibers as a model system of cylindrical porous particles with infinite length. To this end, polystyrene (PS) nanospheres were synthesized by dispersion polymerization. Detailed synthesis conditions can be found elsewhere [16]. After redispersion of PS nanospheres in ethanol containing polyvinylpyrrolidone (PVP), titanium diisopropoxide bisacetylacetonate (TDIP) and dilute hydrochloric acid solution (0.01 N) were added to prepare spinning solution. During electrospinning, high voltage was applied by metallic nozzle for injection of spinning solution as fibers to SUS collector. After spinning, composite fibers were collected for calcination at 500 °C for 5 hours for removal of PS nanospheres to form porous fibers, which was observed by FE-SEM (FE-SEM, Hitachi-S4700). Detailed synthesis conditions are described in our previous article [17].

2. Synthesis of Macroporous Titania Particles by Emulsion-assisted Self-assembly

Spherical porous titania microparticles were synthesized using emulsion droplets as micro-reactors. PS nanospheres dispersed in ethanol were mixed with TDIP, followed by emulsification in tetradecane containing Abil EM90 as emulsifier using homogenizer. The resulting complex fluid was evaporated at 95 °C by heating for gelation of TDIP to form composite microspheres of PS nanospheres and titania. After calcination at 500 °C, microporous titania microspheres were prepared. Detailed synthesis conditions are described in our previous article [15,18].

3. Degradation of Methylene Blue using Microporous Titania Fibers as Photocatalytic Particles

Macroporous titania fibers were suspended in 50-ml (0.0002 g/ml), followed by 50-ml mixing aqueous methylene blue solution (0.00001 g/ml). After equilibration for 30 minutes under stirring at dark condition, UV light was illuminated for 2 hours. During photocatalytic reaction, samples were taken for regular time intervals for measurement of methylene blue concentration using UV-visible spectrometer (Optizen POP).

RESULTS AND DISCUSSION

Like the previous report, the following reaction-diffusion equation can be obtained from material balance in spatial coordinate using effective diffusivity D_e, to obtain concentration of reactant C(r, t) assuming the first-order kinetics.

$$\frac{\partial C}{\partial t} = \frac{D_e}{r^z}\frac{\partial}{\partial r}\left(r^z\frac{\partial C}{\partial r}\right) - kC \tag{1}$$

Here, the value of z is 2, 1, and 0 in spherical, cylindrical, and Cartesian coordinates, respectively. Usually the sign of the first-order rate constant, k, is positive, whereas it can be negative for generating chemical species such as autocatalytic reaction. For nondimensionalization of the differential equation, characteristic time t_c can be defined as R^2/D_e to obtain a more convenient form in the following manner. R can be the radius of spherical particles or cylindrical catalyst, whereas 2R should be the thickness of the slab in rectangular-shaped catalytic film.

$$\frac{\partial y}{\partial \tau} = \frac{1}{x^z}\frac{\partial}{\partial x}\left(x^z\frac{\partial y}{\partial x}\right) - \phi^2 y \tag{2}$$

Here, Thiele modulus ϕ is an important factor since the value of ϕ affects the dimensionless concentration of reactant, y. Our goal was to get an analytical solution y(x, τ) of the above equation as a function of dimensionless radial distance x and dimensionless time τ when the following symmetric boundary condition is applied at the center of the catalytic particle.

$$\text{Boundary condition \#1: } \frac{\partial y}{\partial x} = 0 \text{ at } x=0 \tag{3}$$

Initially, empty catalytic particles should be subject to the initial condition, y(x, 0)=0 and the boundary condition at the catalyst surface can be described as convective condition using Biot number in a different manner for three types of coordinates.

1. Spherical Catalytic Particles

Spherical porous particles are often adopted as catalytic supports or photocatalysts for various chemical reactions [18]. When the mass transfer coefficient of reactant from bulk to the particle is k_L, the boundary condition at the particle surface can be written as follows.

$$-D_e\left(\frac{\partial C}{\partial r}\right)_{r=R} = k_L[C(R, t) - C_b(t)] \tag{4}$$

Here, $C_b(t)$ is time dependent concentration of reactant in bulk phase. More convenient form of the above equation can be obtained in the following manner after nondimensionalization.

$$-\left(\frac{\partial y}{\partial x}\right)_{x=1} = Bi[y(x, \tau) - y_b(\tau)] \tag{5}$$

Here, Biot number can be defined in the following manner, which means the ratio of mass transfer resistance inside solid particles relative to bulk fluid phase.

$$\mathrm{Bi}=\frac{k_L R}{D_e}=\frac{R/D_e}{1/k_L} \tag{6}$$

In this study, the dimensionless bulk concentration, y_b was assumed to decay exponentially as a function of time in the following manner.

$$y_b(\tau)=\exp(-a\tau) \tag{7}$$

The time constant, 1/a, can be measured experimentally from the bulk fluid phase by measuring the concentration of reactant for various reactions [19].

The reaction diffusion Eq. (2) subject to boundary and initial conditions described previously can be solved analytically using eigenfunction expansion method. As described in our previous report, the solution y(x, τ) can be assumed as the summation of the functions $Y^*(x, \tau)$, $R^*(\tau)$, and u(x) in the following manner.

$$y(x, \tau)=Y^*(x, \tau)+R^*(\tau)u(x) \tag{8}$$

By substituting the above expression into the reaction-diffusion equation, the following differential equation and boundary conditions can be obtained.

$$\frac{\partial y}{\partial \tau}=\frac{\partial Y^*}{\partial \tau}+\frac{dR^*}{d\tau}u=\frac{1}{x^2}\frac{\partial}{\partial x}\left(x^2\frac{\partial Y^*}{\partial x}\right)+R^*\frac{1}{x^2}\frac{d}{dx}\left(x^2\frac{du}{dx}\right)-\phi^2Y^*-\phi^2R^*u \tag{9}$$

$$\text{Boundary Conditions: } \frac{\partial Y^*}{\partial x}=0,\ R^*\frac{du}{dx}=0 \text{ (at x=0)} \tag{10}$$

$$\text{and } \left(\frac{\partial Y^*}{\partial x}\right)_{x=1}+\mathrm{Bi}Y^*(1, \tau)+R^*(\tau)\left[\left(\frac{du}{dx}\right)_{x=1}+\mathrm{Biu}(1)\right]$$
$$=\mathrm{Bi}\exp(-a\tau) \text{ (at x=1)} \tag{11}$$

$$\text{Initial Conditions: } Y^*(x, 0)+R^*(0)u(x)=0 \text{ (at } \tau=0) \tag{12}$$

For convenience, u(x) can be defined as steady-state concentration subject to the following convective boundary condition at constant bulk concentration.

$$\frac{1}{x^2}\frac{d}{dx}\left(x^2\frac{du}{dx}\right)-\phi^2u=0 \tag{13}$$

Boundary Conditions:

$$\frac{du}{dx}=0 \text{ (at x=0) and } \left(\frac{du}{dx}\right)_{x=1}+\mathrm{Biu}(1)=\mathrm{Bi} \text{ (at x=1)} \tag{14}$$

The above ordinary differential equation can be solved easily to get the following concentration profile as a function of x and variable parameter Bi.

$$u(x)=\frac{\mathrm{Bi}}{(\mathrm{Bi}-1)\sinh\phi+\phi\cosh\phi}\frac{\sinh(\phi x)}{x} \tag{15}$$

As Bi→∞, the limiting case of the above equation becomes the well-known steady-state concentration of the reactant inside porous spherical catalyst subject to constant surface concentration, u(x)= $\frac{\sinh(\phi x)}{x\sinh(\phi)}$ [20]. Average concentration inside the catalytic particles, $\bar{u}$ can be calculated according to the following integration,

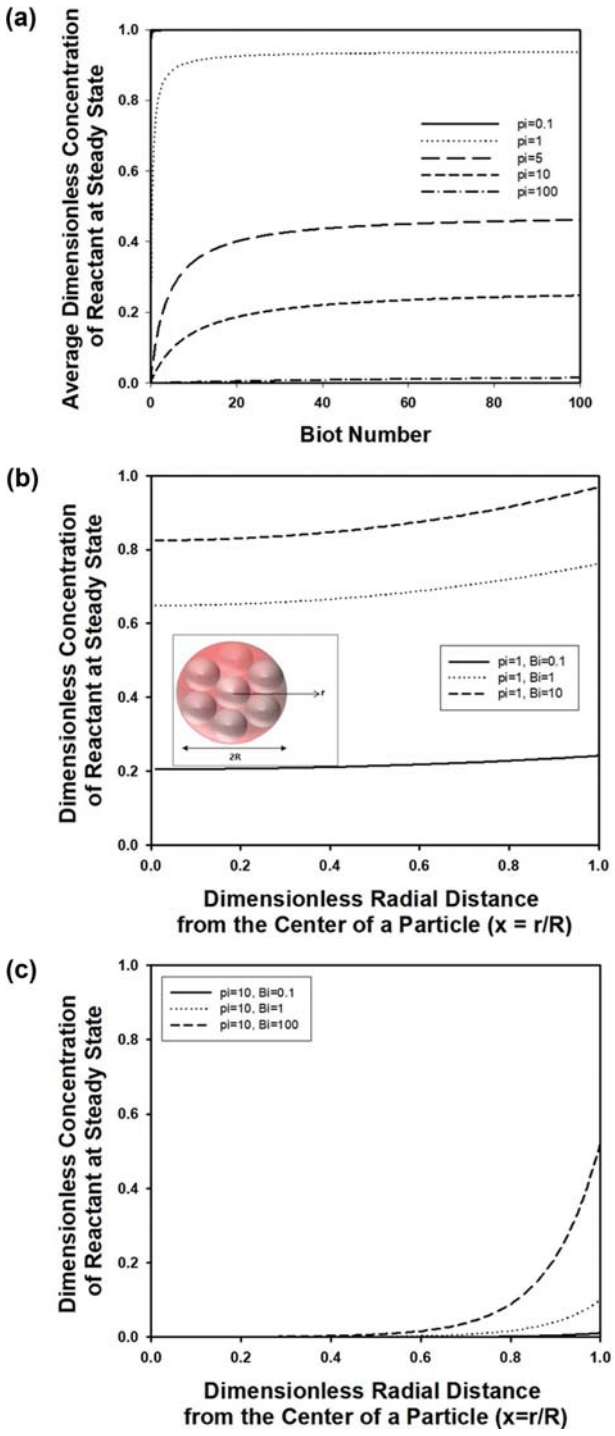

Fig. 1. (a) Dimensionless concentration of reactant at steady state inside spherical porous particle as a function of Biot number (Bi) for Thiele modulus ϕ=0.1, 1, 5, 10, and 100. (b) and (c) Concentration profile of reactant at steady state inside porous particles as a function of radial distance from the center of particle for Bi=0.1, 1, and 10 when ϕ is fixed as 1 and 10, respectively. In inset figure of Fig. 1(b), spherical porous particle is drawn as schematic figure.

and the results depending on Biot number are shown as a graph in Fig. 1(a) for different values of Thiele modulus, ϕ.

$$u = 3\int_0^1 x^2 u(x)dx = \frac{3Bi}{(Bi-1)\sinh\phi + \phi\cosh\phi}\left(\frac{\cosh\phi}{\phi} - \frac{\sinh\phi}{\phi^2}\right) \quad (16)$$

As shown in the graph, the average concentration increased with increasing Biot number, indicating that larger internal mass transfer resistance resulted in the delayed mass transport of the reactant to the central region of porous material. Thus, decomposition of reactant was rarely expected, causing increase of the reactant concentration, as displayed in the graph of Fig. 1(a). However, the concentration of reactant became saturated when Biot number was larger than about 20, implying that this value can be considered as infinitely large. When Biot number was larger than 20, steady-state concentration reached to saturated value regardless of the value of Thiele modulus, and further increase of the reactant concentration was not observed with increasing Biot number. Thus, Bi=20 can be considered as a kind of critical value at steady state.

Fig. 1(b) contains the change of steady-state concentration of reactant as a function of dimensionless radial distance x from the center of the particles for various values of Biot number such as Bi=0.1, 1, and 10, when Thiele modulus, ϕ was fixed as 1. When internal mass transfer resistance was negligible (Bi=0.1), almost uniform concentration of reactant was observed regardless of x. However, dimensionless concentration u increased near the surface of the catalytic particles since reaction time was not enough near the interface due to insufficient retention time inside the particles. Similar to Fig. 1(a), larger mass transfer resistance outside of the particles resulted in decrease of Biot number, causing decreased transport of the reactant through the particles. Thus, the dimensionless concentration, u, decreased with decreasing Biot number, as shown in Fig. 1(b). This trend became more clearer when Thiele modulus increased from 1 to 10, as displayed in Fig. 1(c), indicating that larger reaction rate caused decrease of reactant concentration near the center of the particles. For this case, dimensionless concentration near the particle surface increased with increasing Biot number, since increase of internal mass transfer resistance caused accumulation of reactant near the particle surface, as shown in Fig. 1(c).

Until now, steady-state concentration inside spherical porous catalytic particles has been discussed depending on Thiele modulus and Biot number. Transient dimensionless concentration inside particles can be calculated from Eq. (8) by solving Y^* from the following partial differential equation.

$$\frac{\partial Y^*}{\partial\tau} + \frac{dR^*}{d\tau}u(x) = \frac{1}{x^2}\frac{\partial}{\partial x}\left(x^2\frac{\partial Y^*}{\partial x}\right) - \phi^2 Y^* \quad (17)$$

To solve the above equation, the following homogeneous boundary condition can be imposed, assuming that boundary condition (14) is valid.

$$\left(\frac{\partial Y^*}{\partial x}\right)_{x=1} + BiY^*(1,\ \tau) = 0 \quad (18)$$

Thus, $R(\tau)$ can be obtained as $y_b(\tau)$, which was already assumed as $\exp(-a\tau)$. The partial differential equation for $Y^*(x,\ \tau)$ can be determined in more detail as the following non-homogeneous form with homogeneous boundary conditions.

$$\frac{\partial Y^*}{\partial\tau} = \frac{1}{x^2}\frac{\partial}{\partial x}\left(x^2\frac{\partial Y^*}{\partial x}\right) - \phi^2 Y^* + a\exp(-a\tau)\frac{Bi}{(Bi-1)\sinh\phi + \phi\cosh\phi}\frac{\sinh(\phi x)}{x} \quad (19)$$

$$\text{Initial Condition: } Y^*(x,\ 0) = -R^*(0)u(x) = -\frac{Bi}{(Bi-1)\sinh\phi + \phi\cosh\phi}\frac{\sinh(\phi x)}{x} \quad (\text{at } \tau=0) \quad (20)$$

The above partial differential equation can be solved by applying eigenfunction expansion method, since the boundary conditions at x=0 and x=1 are homogeneous. The eigenfunction as $K_n(x)$ satisfying differential operator $\mathrm{L} = \frac{1}{x^2}\frac{d}{dx}\left(x^2\frac{d}{dx}\right) - \phi^2$ satisfies the following eigenvalue equation.

$$\frac{1}{x^2}\frac{d}{dx}\left(x^2\frac{dK_n}{dx}\right) - \phi^2 K_n = -\xi_n^2 K_n \quad (21)$$

$$\text{Boundary Conditions: } \frac{dK_n}{dx} = 0 \ (\text{at x=0}) \quad \text{and} \left(\frac{dK_n}{dx}\right)_{x=1} + BiK_n(1) = 0 \ (\text{at x=1}) \quad (22)$$

The eigenfunction $K_n(x)$ satisfying boundary conditions can be determined as the following function.

$$K_n(x) = \frac{\sin(\sqrt{\xi_n^2 - \phi^2}\,x)}{x} \text{ and } \sqrt{(\xi_n^2 - \phi^2)} = (1-Bi)\tan(\sqrt{\xi_n^2 - \phi^2}) \quad (23)$$

The eigenvalue ξ_n can be determined by defining $\lambda_n = \sqrt{\xi_n^2 - \phi^2}$ from the following nonlinear equation for various values of Thiele modulus and Biot number.

$$\lambda_n = (1-Bi)\tan\lambda_n \quad (24)$$

Table 1 summarizes the values of λ_n for various Bi and ϕ obtained by solving the above nonlinear equation by graphical interpretation, and $Y^*(x,\ \tau)$ can be expanded using the following time dependent coefficient $a_n(\tau)$ and eigenfunction as a function of x and

Table 1. Eigenvalues λ_n according to Biot number in spherical coordinates

Bi	λ_1	λ_2	λ_3	λ_4	λ_5	λ_6	λ_7
0.1	0.542	4.516	7.738	10.913	14.073	17.227	20.376
1.1	1.632	4.734	7.867	11.005	14.144	17.285	20.425
5	2.57	5.354	8.303	11.335	14.408	17.503	20.612
10	2.836	5.717	8.659	11.653	14.687	17.748	20.828
100	3.11	6.22	9.331	12.441	15.552	18.663	21.775

parameters such as ξ_n and ϕ.

$$Y^*(x,\tau)=\sum_{n=1}^{\infty}a_n(\tau)K_n(x)=\sum_{n=1}^{\infty}a_n(\tau)\frac{\sin(\sqrt{\xi_n^2-\phi^2}x)}{x}=\sum_{n=1}^{\infty}a_n(\tau)\frac{\sin(\lambda_n x)}{x} \tag{25}$$

To determine $a_n(\tau)$, the eigenfunction expansion of nonhomogeneous term in Eq. (19) is also required using another time-dependent coefficient $b_n(\tau)$.

$$a\exp(-a\tau)\frac{Bi}{(Bi-1)\sinh\phi+\phi\cosh\phi}\frac{\sinh(\phi x)}{x}=\sum_{n=1}^{\infty}b_n(\tau)K_n(x) \tag{26}$$

Here, $b_n(\tau)$ can be determined by taking inner product with $K_n(x)$ to both sides due to orthogonality condition.

$$b_n(\tau)=\frac{\langle a\exp(-a\tau)\frac{Bi}{(Bi-1)\sinh\phi+\phi\cosh\phi}\frac{\sinh(\phi x)}{x},K_n(x)\rangle}{\langle K_n,K_n\rangle}=a\exp(-a\tau)\frac{\frac{Bi}{(Bi-1)\sinh\phi+\phi\cosh\phi}\langle\frac{\sinh(\phi x)}{x},K_n(x)\rangle}{\langle K_n,K_n\rangle} \tag{27}$$

In the above equation, denominator, $\langle K_n, K_n\rangle$ can be calculated from the following definition of inner product in spherical coordinate by multiplying x^2 and integration from x=0 to 1.

$$\langle K_n,K_n\rangle=\int_0^1 x^2\frac{\sin(\lambda_n x)}{x}\frac{\sin(\lambda_n x)}{x}dx=\frac{1}{2}-\frac{1}{4\lambda_n}\sin(2\lambda_n) \tag{28}$$

For complete determination of $b_n(\tau)$, the integration, $\langle\frac{\sinh(\phi x)}{x},K_n(x)\rangle$ can be performed to get $\frac{\lambda_n^2}{\phi^2+\lambda_n^2}\left[\frac{\phi\cosh\phi\sin\lambda_n}{\lambda_n^2}-\frac{\sin\phi\cos\lambda_n}{\lambda_n}\right]$. Thus, the time-dependent coefficient, $b_n(\tau)$ can be obtained as the following complicated form.

$$b_n(\tau)=4a\exp(-a\tau)\frac{Bi}{(Bi-1)\sinh\phi+\phi\cosh\phi}\frac{\lambda_n(\phi\cosh\phi\sin\lambda_n-\lambda_n\sinh\phi\cos\lambda_n)}{[2\lambda_n-\sin(2\lambda_n)](\phi^2+\lambda_n^2)} \tag{29}$$

To obtain a transient solution y(x, τ), the following first-order nonhomogeneous equation can be solved to obtain $a_n(\tau)$.

$$\frac{da_n(\tau)}{d\tau}+\xi_n^2a_n(\tau)=b_n(\tau) \tag{30}$$

The initial condition of the above differential equation, $a_n(0)$ can be determined from $Y^*(x,0)=\sum_{n=1}^{\infty}a_n(0)K_n(x)=-R^*(0)u(x)$. By applying inner product with $K_n(x)$, the following initial condition can be achieved.

$$a_n(0)=\frac{\langle -u(x),K_n(x)\rangle}{\langle K_n(x),K_n(x)\rangle}=\frac{-4Bi}{(Bi-1)\sinh\phi+\phi\cosh\phi}\frac{\lambda_n(\phi\cosh\phi\sin\lambda_n-\lambda_n\sinh\phi\cos\lambda_n)}{[2\lambda_n-\sin(2\lambda_n)](\phi^2+\lambda_n^2)} \tag{31}$$

From Eqs. (30) and (31), $a_n(\tau)$ can be obtained as the following complicated form.

$$a_n(\tau)=\frac{4Bi}{(Bi-1)\sinh\phi+\phi\cosh\phi}\left[\frac{\lambda_n(\lambda_n\sinh\phi\cos\lambda_n-\phi\cosh\phi\sin\lambda_n)}{[2\lambda_n-\sin(2\lambda_n)](\phi^2+\lambda_n^2-a)}-\frac{a\lambda_n(\lambda_n\sinh\phi\cos\lambda_n-\phi\cosh\phi\sin\lambda_n)}{[2\lambda_n-\sin(2\lambda_n)](\phi^2+\lambda_n^2)(\phi^2+\lambda_n^2-a)}\right] \tag{32}$$

Now, the transient solution, y(x, τ) can be expressed as the following eigenfunction expansion form.

$$y(x,\tau)=\sum_{n=1}^{\infty}\frac{4Bi}{(Bi-1)\sinh\phi+\phi\cosh\phi}\frac{\lambda_n(\lambda_n\sinh\phi\cos\lambda_n-\phi\cosh\phi\sin\lambda_n)}{[2\lambda_n-\sin(2\lambda_n)](\phi^2+\lambda_n^2-a)}\exp[-(\lambda_n^2+\phi^2)\tau]\frac{\sin(\lambda_n x)}{x}-\sum_{n=1}^{\infty}\frac{4Bi}{(Bi-1)\sinh\phi+\phi\cosh\phi}\frac{a\lambda_n(\lambda_n\sinh\phi\cos\lambda_n-\phi\cosh\phi\sin\lambda_n)}{[2\lambda_n-\sin(2\lambda_n)](\phi^2+\lambda_n^2-a)(\phi^2+\lambda_n^2)}\exp(-a\tau)\frac{\sin(\lambda_n x)}{x}+\exp(-a\tau)\frac{Bi}{(Bi-1)\sinh\phi+\phi\cosh\phi}\frac{\sin(\phi x)}{x} \tag{33}$$

Since only a few important terms contribute to y(x, τ) in the above series solution, we evaluated eigenvalues from n=1 to 7 in Table 1.

Applying transient concentration inside spherical porous particles in Eq. (33), the concentration profile at initial stage of catalytic reaction (τ=0.5) is shown in the graph of Fig. 2(a). The concentration is drawn as a function of x under fixed value of a=1 and Bi=5 for various values of ϕ such as 0.05, 0.5, 2, and 5. For relatively small value of Thiele modulus (ϕ=0.05 and 0.5), the dimensionless concentration increased slightly near the central region of the catalytic particles, since diffusional mass transport to the center of the particle was fast enough to compensate the decrease of reactant concentration due to irreversible reaction. However, the concentration of reactant decreased as *x* approached to 0 when Thiele modulus increased to 2 or 5, because reaction rate became fast to remove reactant molecules, as shown in Fig. 2(a).

Fig. 2(b) contains concentration profile of reactant inside spherical particle for various values of dimensionless time, τ=0.5, 1.5, 2.5, and 5, when Thiele modulus (ϕ), Biot number (Bi), and a were fixed as 2, 5, and 1, respectively. As dimensionless time increased, concentration of reactant decreased due to prolonged reaction time. When τ reached 5, concentration of reactant decreased to almost 0 for every position inside the spherical particles.

Fig. 2(c) contains the effect of Biot number on concentration profile of reactant, when ϕ, a, and τ were fixed as 5, 5, and 1, respectively. As Biot number increased, concentration near particle surface increased due to the decrease of mass transfer resistance from bulk fluid phase to the particle. However, dimensionless concentration decreased as dimensionless radial distance x approached to the center of the spherical particle due to depletion of reactant by irreversible reaction.

The average concentration inside the spherical catalytic particles is also important for investigating the effect of various parameters on reaction. It can be defined as a function of τ in spherical coordinate in the following manner, and calculation is possible after integration.

$$\begin{aligned}\bar{y}(\tau)&=3\int_0^1 x^2y(x,\tau)dx\\&=3\sum_{n=1}^{\infty}\frac{4Bi}{(Bi-1)\sinh\phi+\phi\cosh\phi}\frac{\lambda_n(\lambda_n\sinh\phi\cos\lambda_n-\phi\cosh\phi\sin\lambda_n)}{[2\lambda_n-\sin(2\lambda_n)](\phi^2+\lambda_n^2-a)}\left(\frac{\sin\lambda_n}{\lambda_n^2}-\frac{\cos\lambda_n}{\lambda_n}\right)\exp[-(\lambda_n^2+\phi^2)\tau]\\&\quad-3\sum_{n=1}^{\infty}\frac{4Bi}{(Bi-1)\sinh\phi+\phi\cosh\phi}\frac{a\lambda_n(\lambda_n\sinh\phi\cos\lambda_n-\phi\cosh\phi\sin\lambda_n)}{[2\lambda_n-\sin(2\lambda_n)](\phi^2+\lambda_n^2-a)(\phi^2+\lambda_n^2)}\left(\frac{\sin\lambda_n}{\lambda_n^2}-\frac{\cos\lambda_n}{\lambda_n}\right)\exp(-a\tau)\\&\quad+3\exp(-a\tau)\frac{Bi}{(Bi-1)\sinh\phi+\phi\cosh\phi}\left(\frac{\cosh\phi}{\phi}-\frac{\sinh\phi}{\phi^2}\right)\end{aligned} \tag{34}$$

Fig. 3(a) contains the change of average dimensionless concentration inside the particles as a function of dimensionless reaction time for various Thiele modulus ϕ=0.05, 5, and 75, when a and Bi

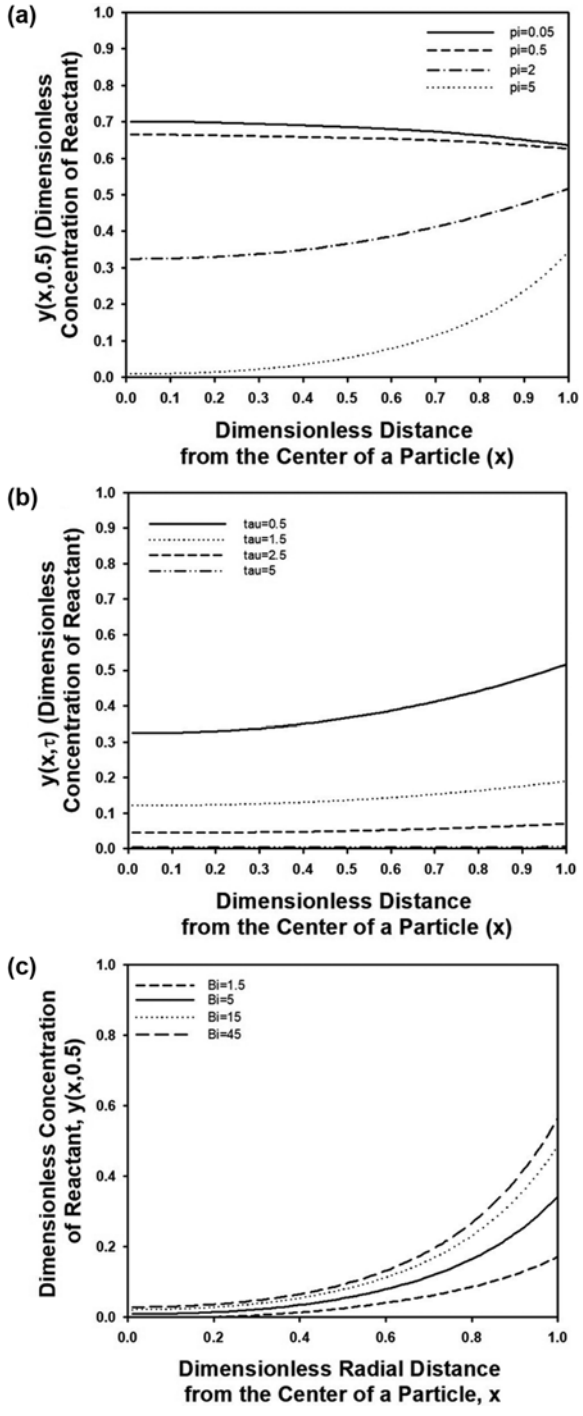

Fig. 2. (a) Concentration profile of reactant inside spherical porous particle as a function of radial distance from the center of particle. Dimensionless reaction time (τ) was fixed as 0.5, while Bi and a were fixed as 5 and 1, respectively. ϕ was adjusted as 0.05, 0.5, 2, and 5 for comparison of the profile. (b) Concentration profile of reactant inside spherical porous particle as a function of radial distance from the center of particle. Bi, ϕ, and a were fixed as 5, 2, and 1, respectively, when τ was adjusted as 0.5, 1.5, 2.5, and 5, respectively. (c) Concentration profile of reactant inside spherical porous particle as a function of radial distance from the center of particle. τ, ϕ, and a were fixed as 0.5, 5, and 1, respectively. Bi was adjusted as 1.5, 5, 15, and 45 for comparison of the profile.

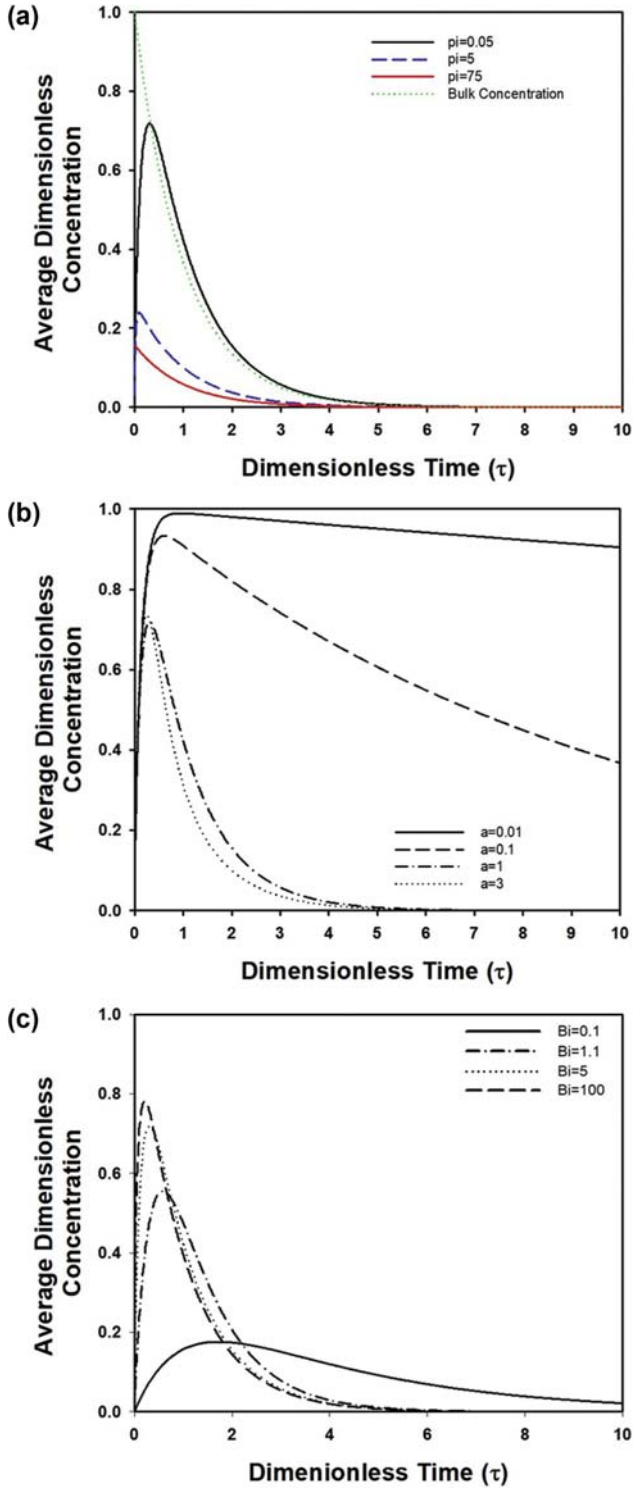

Fig. 3. (a) Average dimensionless concentration $\bar{y}(\tau)$ inside spherical porous particle as a function of dimensionless time τ for a=1 and Bi=5. ϕ was adjusted as 0.05, 5, and 75, respectively. (b) Average dimensionless concentration $\bar{y}(\tau)$ inside spherical porous particle as a function of dimensionless time τ for ϕ=0.05 and Bi=5. a was adjusted as 0.01, 0.1, 1, and 3, respectively. (c) Average dimensionless concentration $\bar{y}(\tau)$ inside spherical porous particle as a function of dimensionless time τ for a=1 and ϕ=0.05. Bi was adjusted as 0.1, 1.1, 5, and 100, respectively.

are fixed as 1 and 5, respectively. Since the catalytic particles were initially empty, the average concentration increased from 0 to maximum value, followed by consistent decrease of the concentration due to first order irreversible reaction. During initial stage of reaction, the increase of reactant concentration was caused by inward diffusional flux of reactant from bulk to the particle, whereas the depletion of the reactant molecule was not sufficient in the early stage of the reaction. The maximum value of the reactant concentration decreased with increasing reaction rate or Thiele modulus due to fast removal of reactant inside the particle, and the required time at maximum concentration (t_{max}) also decreased with increasing Thiele modulus.

The effect of time constant, 1/a on the concentration in bulk fluid phase is shown in Fig. 3(b), which was obtained by fixing the value of Bi and ϕ as 5 and 0.05, respectively. When a was close to 0, the average dimensionless concentration decreased very slowly after temporary rise, since retardation of the decrease of bulk concentration occurred with large time constant. However, decreasing rate of reactant concentration increased drastically with increasing value of a, indicating that the decreasing trend of reactant concentration inside catalytic particles followed the decaying aspect of bulk concentration.

The average dimensionless concentration inside the particles is also drawn in Fig. 3(c) as a function of dimensionless reaction time, for various values of Biot number (Bi=0.1, 1.1, 5, and 100) after fixing other parameters such as a and ϕ as 1 and 0.05, respectively. As Bi increased, maximum average concentration increased, whereas t_{max} decreased. Since reactant molecules accumulate near the particle surface due to large mass transfer resistance inside the catalytic particles, conversion of the reactant by irreversible first-order reaction is rarely expected, causing large maximum reactant concentration with increasing Biot number.

2. Comparison with the Results from Other Geometries such as Cylinder or Slab-type Catalytic Particles

In addition to spherical particles, cylindrical catalytic pellets or slab-type catalyst can be adopted for catalytic reaction. For instance, cylindrical pellets with infinite length and very small diameter can be considered as nanowires or nanofibers, which may have catalytic activity depending on their composition [21]. Slab-type catalytic materials can be adopted as the form of film contacting fluid phase to activate various chemical reactions [22].

In cylindrical coordinates, reaction-diffusion equation can be derived from material balance as the following dimensionless form (z=1 in Eq. (2)).

$$\frac{\partial y}{\partial \tau}=\frac{1}{x}\frac{\partial}{\partial x}\left(x\frac{\partial y}{x}\right)-\phi^2 y \tag{35}$$

Here, the definition of Thiele modulus is the same as that in spherical coordinate. At steady state, the solution u(x) of the above differential equation can be obtained from the following ordinary differential equation subject to proper boundary conditions under constant bulk concentration.

$$\frac{1}{x}\frac{d}{dx}\left(x\frac{du}{dx}\right)-\phi^2 y=0,\ \left(\frac{du}{dx}\right)_{x=0}=0 \text{ and } \left(\frac{du}{dx}\right)_{x=1}+Biu(1)=Bi \tag{36}$$

u(x) can be easily obtained as the following modified Bessel function with order 0, affected by two parameters such as Biot number and Thiele modulus.

$$u(x)=\frac{BiI_0(\phi x)}{BiI_0(\phi)+\phi I_1(\phi)} \tag{37}$$

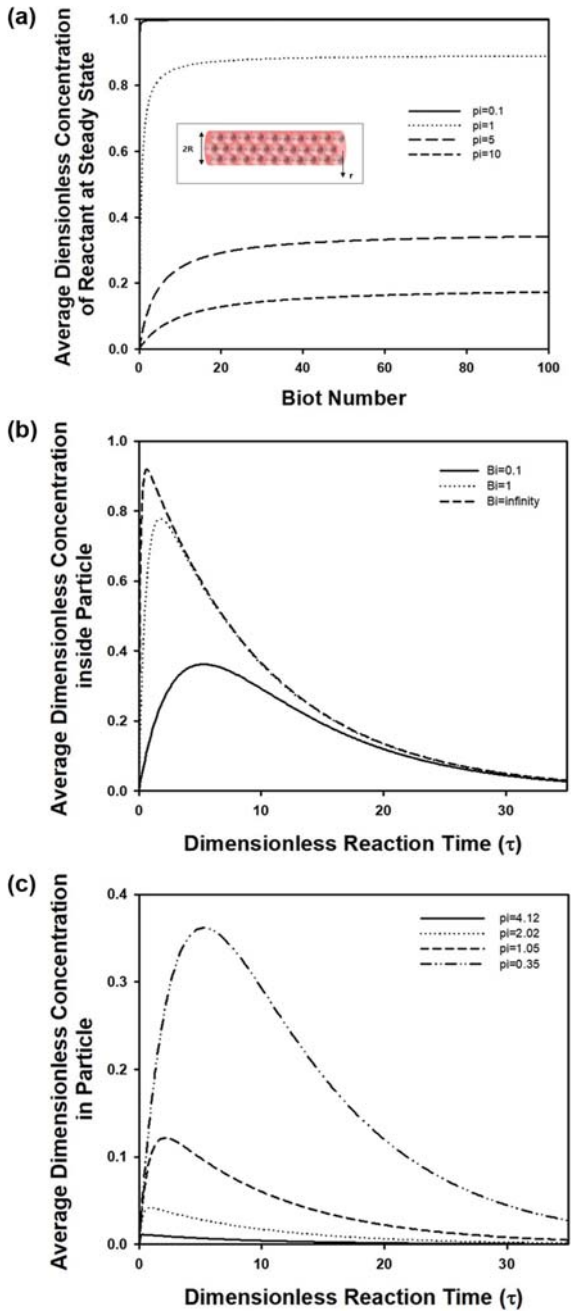

Fig. 4. (a) Dimensionless concentration of reactant at steady state inside cylindrical porous particle as a function of Bi for ϕ=0.1, 1, 5, and 10. In the inset Fig. 4(a), cylindrical porous particle is drawn as schematic. (b) Average dimensionless concentration $\bar{y}(\tau)$ inside cylindrical porous particle as a function of dimensionless time τ for a=0.1 and ϕ=0.35. Bi was adjusted as 0.1, 1, and infinity, respectively. (c) Average dimensionless concentration $\bar{y}(\tau)$ inside cylindrical porous particle as a function of dimensionless time τ for a=1 and Bi=0.1. ϕ was adjusted as 0.35, 1.05, 2.02, and 4.12, respectively.

Fig. 4(a) contains steady-state dimensionless average concentration of reactant inside cylindrical particles as a function of Biot number for various values of Thiele modulus, ϕ=0.1, 1, 5, and 10, assuming constant bulk concentration. Similar to spherical particles, the reactant concentration inside particles increased with increasing Biot number, and saturation behavior was observed when Biot number was larger than about 20. When the value of Thiele modulus decreased, average concentration at steady-state was almost the same as the initial concentration due to negligible reaction rate.

As explained in Supporting Information, transient concentration y(x, τ) inside cylindrical particle can be obtained by Laplace transform method. The average concentration $\bar{y}(\tau)$ in cylindrical particles can be calculated from the following definition.

$$\bar{y}(\tau)=2\int_0^1 x^2 y(x,\tau)dx$$
$$=2\exp(-a\tau)\frac{I_1(\sqrt{\phi^2-a})}{\sqrt{\phi^2-a}\left[I_0(\sqrt{\phi^2-a})+\frac{\sqrt{\phi-a}}{Bi}I_1(\sqrt{\phi^2-a})\right]} \quad (38)$$
$$-4\sum_{n=1}^{\infty}\frac{J_1(\lambda_n)}{(\lambda_n^2+\phi^2-a)\left[J_1(\lambda_n)+\frac{\lambda_n}{Bi}J_0(\lambda_n)\right]}\exp[-(\lambda_n^2+\phi^2)\tau]$$

Here, eigenvalue, λ_n, satisfies the transcendental equation, $\lambda_n J_1(\lambda_n)=BiJ_0(\lambda_n)$, and Table 2 summarizes the various λ_n according to various Biot numbers, which were calculated by graphical method.

Transient behavior of average dimensionless concentration of reactant, $\bar{y}(\tau)$ is plotted in Fig. 4(b), for Biot numbers such as Bi=0.1, 1, and ∞, when ϕ and a are fixed as 0.35 and 0.1, respectively. Like spherical particles, the required time to reach maximum concentration (t_{max}) became shorter with increasing Biot number, and the concentration of reactant inside cylindrical particles decreased to 0 after the reaction proceeded sufficiently. Maximum concentration increased with increasing Biot number, since mass transfer resistance from bulk fluid to particles decreased for larger value of Biot number. When small Biot number (Bi=0.1), t_{max} increased significantly, whereas maximum concentration decreased, compared to the result at larger Biot number (Bi=1). When Biot number and a were fixed as 0.1, maximum concentration of reactant inside cylindrical particles decreased with increasing Thiele modulus from ϕ=0.35 to 4.12 due to depletion of reactant under higher reaction rate, as shown in Fig. 4(c).

In an experiment, infinitely long cylindrical porous particles can be prepared as the form of porous fibers by electrospinning using various precursor materials. In this study, macroporous titania fibers with uniform thickness (R=0.25 μm) could be synthesized using TDIP as precursor and PS nanospheres as templating materials by electrospinning. As shown in the SEM image of Fig. 5(a), the micro-structure of the cylindrical porous fibers could be observed, although it is difficult to confirm their inner structure from the surface image. However, porous morphology could be observed from inset SEM image containing the cross-section of the fibrous material, where spherical air cavities formed porous architecture. Since the polystyrene nanospheres were removed during calcination at 500 °C, spherical macropores were created as displayed in the inset SEM image of Fig. 5(a), to form porous titania fibers, which is advantageous to increase specific surface area.

Since photocatalytic activity can be expected from the macroporous titania fibers, photocatalytic decomposition reaction of methylene blue was carried out from aqueous medium under UV illumination using the porous fibers as cylindrical porous catalytic particles. Although the change of reactant concentration can be measured experimentally using UV-visible spectrometer during reaction, as shown in the data of Fig. 5(b) and 5(c), the concentration of reactant can be calculated from Eq. (38) by assuming Biot number as Bi=0.1 or ∞. Since apparent rate constant of decomposition reaction, k_{app} could be estimated as 0.016 min^{-1} from experimental data of reactant concentration from aqueous medium, Thiele modulus was predicted as $\phi=R\sqrt{\frac{k_{app}}{D_e}}$ using effective diffusivity inside porous medium. Like the previous paper, the parameter, a in Eq. (38) can be also estimated by $a=\frac{R^2\lambda}{D_e}$ using adsorption rate constant λ, which was measured as 0.00165 sec^{-1} by other groups [15,23]. To apply these parameters for the prediction of reactant concentration inside particles, effective diffusivity, D_e ($=D\varepsilon_p/\tau_t$) can be calculated by multiplying the ratio of porosity of porous particles (ε_p) and tortuosity (τ_t) with diffusion coefficient of methylene blue, D in aqueous medium, which can be obtained from other literature as $D=4.5\times10^{-10}$ m^2/s [24]. In Fig. 5(b), ε_p/τ_t is fixed as 0.005 and 0.05 for Fig. 5(b) and 5(c), respectively, assuming very high tortuosity, to calculate average concentration of reactant inside cylindrical particles. After initial sharp rise of the concentration, rapid removal of the reactant was predicted inside the particle due to irreversible firs-order reaction. Though the difference between the concentration inside and outside of the particle could be considered as driving force of mass transfer of reactant from bulk to particles, the effect of Biot number was negligible, since predicted values of concentration were almost the same for Bi=0.1 and ∞, as shown in Fig. 5(b). However, the concentration of reactant inside cylindrical particles was affected by Biot number, when

Table 2. Eigenvalues λ_n according to Biot number in cylindrical coordinates

Bi	λ_1	λ_2	λ_3	λ_4	λ_5	λ_6	λ_7
0.1	0.442	3.858	7.03	10.183	13.331	16.477	19.621
1	1.256	4.079	7.156	10.271	13.398	16.531	19.667
5	1.99	4.713	7.618	10.622	13.679	16.763	19.864
10	2.179	5.033	7.957	10.936	13.958	17.01	20.083
100	2.381	5.465	8.568	11.675	14.783	17.893	21.004

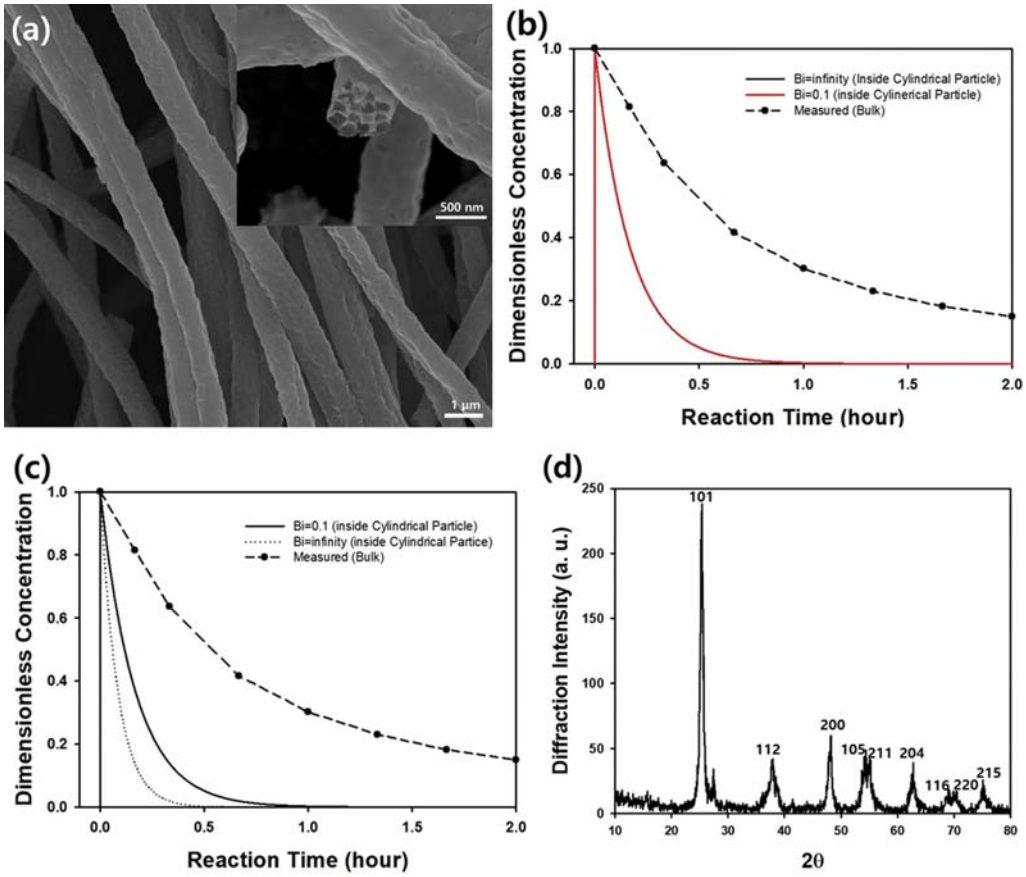

Fig. 5. (a) SEM image of macroporous cylindrical titania fibers used for photocatalytic degradation of methylene blue. Scale bar indicates 1 μm. Inset SEM image shows magnified cross-sectional SEM image of a macroporous titania fiber, and scale bar is 500 nm. (b) and (c) The change of the average concentration of reactant inside the macroporous cylindrical titania particles obtained by the calculation using the analytical solution, when ε_p/τ_t was fixed as 0.005 and 0.05, respectively. The change of the bulk concentration of the reactant measured during photocatalytic decomposition reaction was also included for comparison. (d) Powder XRD analysis result of porous titania fibers shown in Fig. 5(a).

ε_p/τ_t was fixed as 0.05, which is more reasonable value than 0.005. As shown Fig. 5(c), the decreasing rate of reactant became retarded when Biot number decreased from ∞ to 0.1, indicating that increase of internal resistance of mass transfer slowed the transport of reactant through the particles. Since crystalline structure as well as porous morphology may affect the photocatalytic activity of titania material, it is important to confirm the microcrystalline structure of the titania fibers used for experiments. In Fig. 5(d), the crystalline structure of titania fibers in Fig. 5(a) is contained as powder XRD analysis result, which is quite close to anatase crystal structure in JCPDS card no. 21-1272) [25]. Though further heating of the sample at 1,000 °C may induce rutile crystal, macroporous structure of the titania fibers can be deteriorated at higher heating condition.

In addition to cylindrical porous titania particles, spherical porous titania particles were also synthesized to apply photocatalytic particles. As displayed in SEM image of Fig. 6(a), spherical macroporous titania crystallite could be fabricated from emulsion droplets as micro-reactor. Spherical air cavities could be formed inside the porous particles after calcination by removal of PS nanospheres as templates, as displayed in the SEM image. Average particle size was measured as 1.03 μm from the size distribution of the particles in inset histogram of Fig. 6(a). Under UV irradiation, methylene blue was removed using the spherical porous particles as photocatalyst, and the resulting change of the dimensionless concentration of the organic dye was measured as included in experimental data of Fig. 6(b). By assuming the experimental data as the first-order kinetics, apparent rate constant, k_{app}, was estimated as 0.0489 min^{-1}, which was much larger than that of cylindrical porous titania particles. Similar to porous cylindrical titania particles, the necessary parameters such as a and ϕ for calculation of the dye concentration inside the porous spherical particles could be determined as 1.8227×10^{-5} and 0.003, respectively, by assuming ε_p/τ_t was fixed as 0.05. When Biot number was fixed as 0.1, the predicted concentration was plotted as solid line in Fig. 6(b), which is smaller value than bulk concentration of methylene blue measured by experiments. Thus, the difference between the concentration in bulk and inside particles may cause the mass transfer of the dye molecules from reservoir to particles.

When the shape of the catalytic pellet is slab-type, reaction-diffusion equation becomes a more simple form. When z=0 in Eq. (2), eigenfunction expansion method can be applied to obtain the

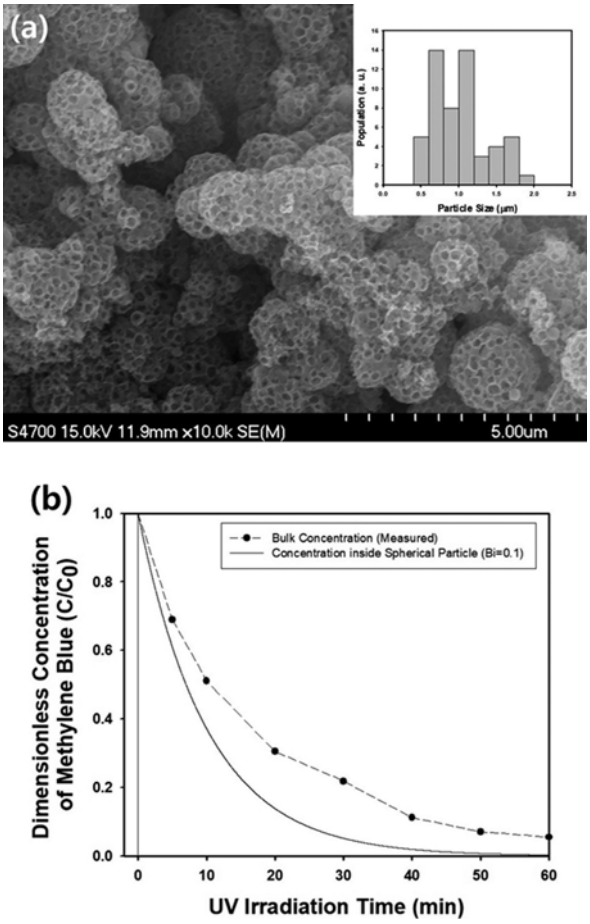

Fig. 6. (a) SEM image of macroporous spherical titania particles used for photocatalytic degradation of methylene blue. Scale bar indicates 5 μm. Inset histogram shows the size distribution of the particles. (b) The change of the average concentration of reactant inside the macroporous spherical titania particles obtained by the calculation using the analytical solution, when ε_p/τ_t and Biot number were fixed as 0.05 and 0.1, respectively. The change of the bulk concentration of the reactant measured during photocatalytic decomposition reaction was also included for comparison.

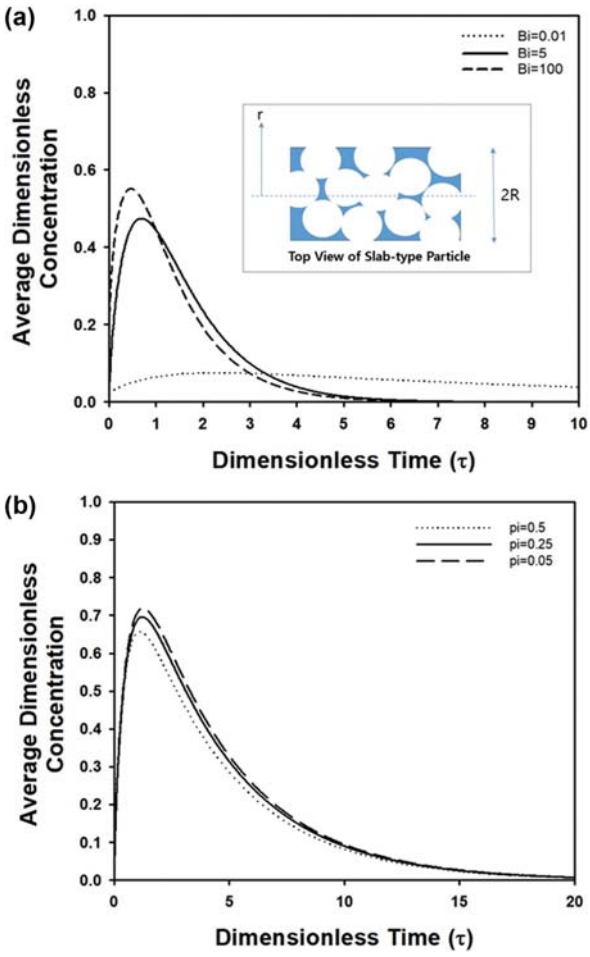

Fig. 7. (a) Average dimensionless concentration $\bar{y}(\tau)$ inside slap-type porous particle as a function of dimensionless time τ for a=1 and ϕ=0.05. Bi was adjusted as 0.1, 5, and 100, respectively. Inset figure shows top views of a porous slab-type particle schematically. (b) Average dimensionless concentration $\bar{y}(\tau)$ inside slab-type porous particle as a function of dimensionless time τ for a=0.25 and Bi=5. ϕ was adjusted as 0.05, 0.25, and 0.5, respectively.

following average dimensionless concentration $\bar{y}(\tau)$ of reactant inside the slab.

$$\bar{y}(\tau)=\frac{1}{\phi}\frac{\mathrm{Bi}\sinh(\phi)}{\mathrm{Bi}\cosh(\phi)+\phi\sinh\phi}\exp(-a\tau)+4\sum_{n=1}^{\infty}\frac{\mathrm{Bi}\sin\lambda_n(\phi^3\cos\lambda_n\sinh\phi+\lambda_n\sin\lambda_n\cos\phi)[a\exp(-a\tau)-\{\phi^2+\lambda_n^2\}\exp\{-(\phi^2+\lambda_n^2)\tau\}]}{(\lambda_n^2+\phi^2-a)(\mathrm{Bi}\cosh\phi+\phi\sinh\phi)[2\lambda_n+\sin(2\lambda_n)](\phi^2+\lambda_n^2)} \quad (39)$$

Here, λ_n denotes eigenvalue which satisfies $\lambda_n/\mathrm{Bi}=\cot\lambda_n$. Table 3 contains eigenvalues in Cartesian coordinates obtained graphically for various value of Biot number.

Fig. 7(a) contains the change of average dimensionless concentration as a function of dimensionless time in slab-type catalytic particles. When Thiele modulus ϕ and a were fixed as 0.05 and 1, respectively, transient behavior of the average concentration changed

Table 3. Eigenvalues λ_n according to Biot number in cartesian coordinates

Bi	λ_1	λ_2	λ_3	λ_4	λ_5	λ_6	λ_7
0.1	0.311	3.173	6.299	9.435	12.574	15.714	18.855
1	0.86	3.426	6.437	9.529	12.645	15.711	18.902
5	1.314	4.034	6.91	9.893	12.935	16.011	19.106
10	1.429	4.306	7.228	10.2	13.214	16.259	19.327
100	1.555	4.666	7.776	10.887	13.998	17.109	20.221

significantly depending on Biot number. When Biot number was a negligible value, the concentration inside the particles was quite small, since small Biot number resulted in large external resistance of mass transfer from fluid phase to particle surface, causing almost empty catalytic particles. However, the average concentration increased to a maximum value and decayed with reaction time when Biot number was large (Bi=100). Fig. 7(b) contains the transient behavior of average concentration inside slab-type catalytic particles when Biot number and a were fixed as 5 and 0.25, respectively. For intermediate value of Biot number, the maximum average concentration was not affected seriously by increase of Thiele modulus ϕ=0.05 to 0.5. In these cases, the changing trend was quite similar, since time constant 1/a in bulk concentration was smaller than that of Fig. 7(a).

3. Approximate Solutions of Transient Concentration in Slurry-type Batch Photocatalytic Reactor Containing Spherical Porous Photocatalytic Particles from Coupled Differential Equations

To predict transient bulk concentration of reactant in slurry-type batch photocatalytic reactor, coupled differential equations on the concentration of the reactant inside photocatalytic particles and bulk phase, c_p and c_b, respectively, should be solved simultaneously. The particles can be assumed as spherical morphologies without inert core. Unlike a conventional catalytic reaction, a photocatalytic reaction proceeds inside the porous particles and bulk fluid phase simultaneously, yielding the following governing equations for spherical particles.

$$\varepsilon_p\frac{\partial c_p}{\partial t}=D_e\frac{1}{r^2}\frac{\partial}{\partial r}\left(r^2\frac{\partial c_p}{\partial r}\right)-kc_p$$
$$\text{subject to } c_p(r,\,o)=0,\ \left(\frac{\partial c_p}{\partial r}\right)_{r=0}=0 \text{ and } D_e\left(\frac{\partial c_p}{\partial r}\right)_{r=R}=k_f[c_b-c_p(R,\,t)] \tag{40}$$

$$\frac{dc_b}{dt}=-\frac{1}{V}\frac{m_p}{\rho_p}\frac{3}{R}D_e\left(\frac{\partial c_p}{\partial r}\right)_{r=R}-kc_b \text{ subject to } c_b(0)=c_0 \tag{41}$$

In the above equation, V is the volume of reactor, whereas m_p and ρ_p are the added amount (weight) and density of catalytic particles, respectively. ε_p and k_f denote porosity of the particles and mass transfer coefficient between bulk phase and particle surface, respectively. The first-order rate constant, k was assumed as the same value inside the particles and bulk fluid phase. Here, (3/R)(1/V)(m_p/ρ_p) means total surface area of particle suspension inside the reactor, which is adjustable by changing the amount of particulate materials before start-up. Material property of catalytic particles also affects the value of particle density, diffusivity, and reaction rate. Eqs. (40) and (41) can be nondimensionalized in the following manner by defining characteristic time, t_c and Thiele modulus, ϕ as $\frac{R^2}{D_e}\varepsilon_p$ and $\frac{kR^2}{D_e}\varepsilon_p$, respectively.

$$\frac{\partial y_p}{\partial\tau}=\frac{1}{x^2}\frac{\partial}{\partial x}\left(x^2\frac{\partial y_p}{\partial x}\right)-\phi^2 y_p \text{ (for sphere)}$$
$$\text{subject to } y_p(x,\,o)=0,\ \left(\frac{\partial y_p}{\partial x}\right)_{x=0}=0 \text{ and } \left(\frac{\partial y_p}{\partial x}\right)_{x=1}+Biy_p(1,\,\tau)=y_b(1,\,\tau) \tag{42}$$

$$\frac{dy_b}{d\tau}=-\frac{3\varepsilon_p}{V}\frac{m_p}{\rho_p}\left(\frac{\partial y_p}{\partial x}\right)_{x=1}-\phi^2 y_b \text{ subject to } y_b(0)=1 \tag{43}$$

Laplace transform of Eqs. (42) and (43) results in the following equation in Laplace domain.

$$\frac{1}{x^2}\frac{d}{dx}\left(x^2\frac{dY_p}{dx}\right)-(\phi^2+s)Y_p=0$$
$$\text{subject to } \left(\frac{dY_p}{dx}\right)_{x=0}=0 \text{ and } \left(\frac{dY_p}{dx}\right)_{x=1}+BiY_p(1,\,s)=BiY_b(s) \tag{44}$$

$$sY_b(s)-1=-\frac{3\varepsilon_p}{V}\frac{m_p}{\rho_p}\left(\frac{\partial y_p}{\partial x}\right)_{x=1}-\phi^2 Y_b(s) \tag{45}$$

Applying symmetric boundary condition, the above coupled ordinary differential equations can be solved to obtain $Y_p(x,\,s)$ and $Y_b(s)$ using undetermined coefficient A(s).

$$Y_p(x,\,s)=A(s)\frac{\sinh(\sqrt{\phi^2+s}\,x)}{x} \text{ and}$$
$$Y_b(s)=\frac{1}{\phi^2+s}-A(s)\frac{3\varepsilon_p}{V}\frac{m_p}{\rho_p}\frac{\sqrt{\phi^2+s}\cosh(\sqrt{\phi^2+s})-\sinh(\sqrt{\phi^2+s})}{\phi^2+s} \tag{46}$$

Since it is very difficult to obtain the inverse Laplace transform for a general value of Biot number, the result for Bi$\to\infty$ was only considered in this article. For this case, the convective boundary condition can be simplified as $Y_p(1,\,s)=Y_b(s)$ in Laplace domain, yielding the following equation of A(s).

$$A(s)=\frac{1}{\frac{3\varepsilon_p}{V}\frac{m_p}{\rho_p}\sqrt{\phi^2+s}\cosh(\sqrt{\phi^2+s})-\sinh(\sqrt{\phi^2+s})+(\phi^2+s)\sinh(\sqrt{\phi^2+s})} \tag{47}$$

Thus, $Y_b(s)$ can be determined completely as the following manner, although the inverse transform may not be easily obtained.

$$Y_b(s)=\frac{1}{\phi^2+s}-\frac{1}{1+\frac{1}{\frac{3\varepsilon_p}{V}\frac{m_p}{\rho_p}[\sqrt{\phi^2+s}\coth(\sqrt{\phi^2+s})-1]}\frac{\phi+s}{\phi^2+s}}\frac{1}{\phi^2+s} \tag{48}$$

The right hand side of the above equation can be rearranged to apply infinite geometric series, since $\frac{\sqrt{\phi^2+s}\coth(\sqrt{\phi^2+s})-1}{\phi^2+s}$ is always smaller than 3.

$$\begin{aligned}Y_b(s)&=\frac{1}{\phi^2+s}\frac{1}{1+3\left(\frac{m_p/\rho_p}{V}\varepsilon_p\right)\frac{\sqrt{\phi^2+s}\coth(\sqrt{\phi^2+s})-1}{\phi^2+s}}\\&=\frac{1}{\phi^2+s}\left[1-3\frac{m_p/\rho_p}{V}\varepsilon_p\frac{\sqrt{\phi^2+s}\coth(\sqrt{\phi^2+s})-1}{\phi^2+s}\right.\\&\quad\left.+\left(3\frac{m_p/\rho_p}{V}\varepsilon_p\frac{\sqrt{\phi^2+s}\coth(\sqrt{\phi^2+s})-1}{\phi^2+s}\right)^2-+\cdots\right]\end{aligned} \tag{49}$$

As approximate solution, the first and second terms of the above equation can be considered as the most important contributions, since $\frac{m_p/\rho_p}{V}$ is quite small value in slurry-type reactor using dilute suspension. Since the inverse transform of $\frac{1}{s}\frac{\sqrt{s}\coth(\sqrt{s})-1}{s}=\frac{1}{s}\left(\frac{\coth(\sqrt{s})}{\sqrt{s}}-\frac{1}{s}\right)$ can be obtained as $\int_0^\tau\frac{1}{\sqrt{\pi t}}\left[1+2\sum_{n=1}^{\infty}\exp\left(-\frac{n^2}{t}\right)\right]$

dt$-\tau$ by convolution theorem, the approximate solution of $y_b(\tau)$ can be calculated after applying s-shifting theorem [15,26]. The integral term can be calculated by proper substitution of variable and integration by part, yielding the following approximate solution, which can be applied to dilute particulate suspension.

$$y_b(\tau) \cong \exp(-\phi^2\tau) - 3\frac{m_p/\rho_p}{V}\varepsilon_p \exp(-\phi^2\tau)\left[\int_0^{\tau}\frac{1}{\sqrt{\pi t}}\left\{\left[1+2\sum_{n=1}^{\infty}\exp\left(-\frac{n^2}{t}\right)\right]\right\}dt - \tau\right]$$
$$= \exp(-\phi^2\tau) - 3\frac{m_p/\rho_p}{V}\varepsilon_p \exp(-\phi^2\tau)\left[2\sqrt{\frac{\tau}{\pi}} + 2\sum_{n=1}^{\infty}\left[\sqrt{\tau}\exp\left(-\frac{n^2}{\tau}\right) + n\sqrt{\pi}\left\{1-\mathrm{erf}\left(\frac{n}{\sqrt{\tau}}\right)\right\}\right] - \tau\right] \quad (50)$$

In the above equation, the complementary error function can be replacing the following approximate function [27].

$$1-\mathrm{erf}\left(\frac{n}{\sqrt{\tau}}\right) \quad (51)$$

$$\cong \frac{1}{\{1+c_1(n/\sqrt{\tau})+c_2(n/\sqrt{\tau})^2+c_3(n/\sqrt{\tau})^3+c_4(n/\sqrt{\tau})^4\}^4}$$

Here, the values of constants such as c_1, c_2, c_3, and c_4 are 0.278393, 0.230389, 0.000972, and 0.078108, respectively.

In batch-mode photocatalytic reactor, light illumination is essential for generation of active components for decomposition of reactant, as shown schematically in Fig. 8(a), and light illumination time can be considered as reaction time, t, which can be calculated by multiplying characteristic time, t_c with τ. t_c can be determined based on physicochemical properties summarized in Table 4. Fig. 8(b) contains the transient bulk concentration ($y_b=C_b/C_0$) of reactant as a function of reaction time, t according to various values of Thiele modulus such as ϕ=0.0102, 0.0204, and 0.0408. Since reaction rate constant increased with increasing Thiele modulus,

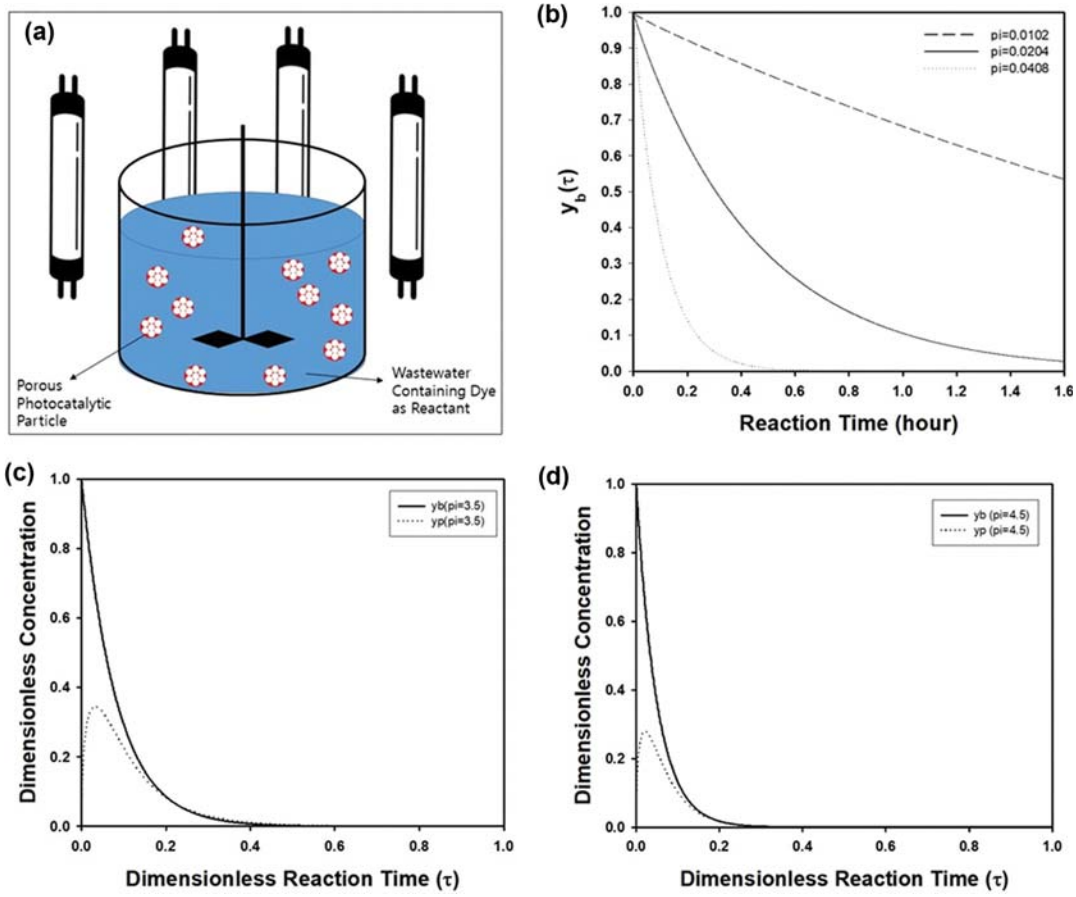

Fig. 8. (a) Schematic figure of batch-mode photocatalytic reactor containing porous catalytic particles. (b) Change of bulk concentration $y_b(\tau)$ in slurry-type batch reactor containing spherical porous photocatalytic particles as a function of reaction time. ϕ was adjusted as 0.0102, 0.0204, and 0.0408, respectively. (c) and (d) Change of average concentration inside spherical porous photocatalytic particle (dotted line) as a function of dimensionless reaction time (τ), when ϕ was adjusted as 3.5 and 4.5, respectively. $y_b(\tau)$ is also plotted for comparison in each graph as solid line.

Table 4. Various parameters for the calculation of bulk concentration and average concentration of reactant inside porous spherical, long cylindrical, or slab-type photocatalytic particles. The parameters written in bold character were adopted from literature

Shape	R	D_e	k_{app}	ϕ
Sphere or cylinder	1.34 μm	2.2767×10^{-12} m^2/s	0.0317 min^{-1}	0.0204125
Slab	1.34 μm	2.2767×10^{-12} m^2/s	0.016 min^{-1}	0.0126

the decreasing rate of bulk concentration increased drastically, as shown in Fig. 8(b).

In addition to bulk concentration, the approximate solution of dimensionless concentration $\overline{y}_p(\tau)$ inside spherical photocatalytic particles can be also found by integrating the $3x^2Y_p(x, \tau)$ from x=0 to 1.

$$\overline{Y}_p(s)=\frac{3}{\phi^2+s}\frac{\frac{\sqrt{\phi^2+s}\coth(\sqrt{\phi^2+s})-1}{\phi^2+s}}{1+3\left(\frac{m_p/\rho_p}{V}\varepsilon_p\right)\frac{\sqrt{\phi^2+s}\coth(\sqrt{\phi^2+s})-1}{\phi^2+s}} \tag{52}$$

$$=\frac{3}{\phi^2+s}\frac{\sqrt{\phi^2+s}\coth(\sqrt{\phi^2+s})-1}{\phi^2+s}\left[1-3\frac{m_p/\rho_p}{V}\varepsilon_p\frac{\sqrt{\phi^2+s}\coth(\sqrt{\phi^2+s})-1}{\phi^2+s}+\left(3\frac{m_p/\rho_p}{V}\varepsilon_p\frac{\sqrt{\phi^2+s}\coth(\sqrt{\phi^2+s})-1}{\phi^2+s}\right)-+\ldots\right]$$

When ϕ=0, the first two terms from the above series solution can be adopted for approximation of infinite series, since $\frac{m_p/\rho_p}{V}\varepsilon_p$ is quite small in diluted suspension.

$$\overline{Y}_p(s)=\frac{3\sqrt{s}\coth(\sqrt{s})-1}{s}\left[1-3\frac{m_p/\rho_p}{V}\varepsilon_p\frac{\sqrt{s}\coth(\sqrt{s})-1}{s}\right] \tag{53}$$

$$=\frac{3\sqrt{s}\coth(\sqrt{s})-1}{s}-9\frac{m_p/\rho_p}{V}\varepsilon_p\left\{\frac{1}{s^2}\coth^2(\sqrt{s})-\frac{2}{s^2\sqrt{s}}\coth(\sqrt{s})+\frac{1}{s^3}\right\}$$

In the above equation, $\left\{\frac{1}{s^2}\coth^2(\sqrt{s})-\frac{2}{s^2\sqrt{s}}\coth(\sqrt{s})\right\}$ is quite small, thus enabling additional approximation. By Applying s-shifting theorem for nonzero-valued ϕ and convolution theorem, the following approximate solution can be obtained after proper integration.

$$\overline{y}_p(\tau)\cong 3\exp(-\phi^2\tau)\left[\int_0^\tau\frac{1}{\sqrt{\pi t}}\left(1+2\sum_{n=1}^{\infty}\exp\left(-\frac{n^2}{t}\right)\right)dt-\tau\right]$$

$$-\frac{9}{2}\frac{m_p/\rho_p}{V}\varepsilon_p\exp(-\phi^2\tau) \tag{54}$$

$$=3\exp(-\phi^2\tau)\left[2\sqrt{\frac{\tau}{\pi}}+2\sum_{n=1}^{\infty}\left\{\sqrt{\tau}\exp\left(-\frac{n^2}{\tau}\right)+n\sqrt{\pi}\left(1-\mathrm{erf}\left(\frac{n}{\sqrt{\tau}}\right)\right)\right\}-\tau\right]$$

$$-\frac{9}{2}\frac{m_p/\rho_p}{V}\varepsilon_p\exp(-\phi^2\tau)$$

Fig. 8(c) contains the transient behavior of bulk concentration, which is compared to the change of average concentration of reactant inside particles for ϕ=3. For prediction, the approximate solutions of Eqs. (50) and (54) were adopted for small values of B= 5.2×10^{-5}, which is reasonable for a diluted suspension in slurry-type photocatalytic reactor. During the drastic decrease of the bulk concentration from $y_b(0)=1$, $\overline{y}_p(\tau)$ increased from 0 to its maximum concentration due to inward flux of reactant from bulk to the spherical porous photocatalytic particles, followed by decaying of the reactant owing to the first-order irreversible reaction. After the dimensionless reaction progressed sufficiently, the decaying trend of $\overline{y}_p(\tau)$ and $y_b(\tau)$ was similar, since depletion of the reactant occurred simultaneously. When Thiele modulus, ϕ increased from 3 to 4.5, half-life of bulk concentration decreased drastically, as displayed in Fig. 8(d). Since reaction rate is proportional to ϕ, maximum average concentration of reactant inside spherical photocatalytic particles also decreased with increasing value of ϕ.

The approximate solutions of transient concentrations are limited to the cases of large Biot numbers and diluted slurry-type photocatalytic reactor. Though more accurate solutions can be obtained numerically, insights on physicochemical phenomena related to reaction-diffusion can be provided from the solutions as formulated form such as Eqs. (50) and (54).

4. Analytical Solutions of Transient Concentration in Slurry-type Batch Photocatalytic Reactor Containing Spherical Porous Photocatalytic Particles from Coupled Differential Equations

When Biot number is very large (Bi→∞), Eqs. (44) and (45) can be solved as the form of trigonometric functions using imaginary number in Laplace domain, as shown in the following manner.

$$Y_p(x, s)=A(s)\frac{\sin(i\sqrt{\phi^2+sx})}{x}$$

$$\text{and } Y_b(s)=\frac{1}{\phi^2+s}-3A(s)\frac{m_p/\rho_p}{V\rho_p}\varepsilon_p[(i\sqrt{\phi+s})\cos(i\sqrt{\phi^2+s})-\sin(i\sqrt{\phi^2+s})] \tag{55}$$

From the boundary condition shown in Eq. (44) at the particle surface, A(s) can be determined in the following form.

$$A(s)=\frac{1}{3\frac{m_p/\rho_p}{V}\varepsilon_p[i\sqrt{\phi^2+s}\cos(i\sqrt{\phi^2+s})-\sin(i\sqrt{\phi^2+s})]+(s+\phi^2)\sin(i\sqrt{\phi^2+s})} \tag{56}$$

Thus, $Y_p(x, s)$ and $Y_b(s)$ have the following form.

$$Y_p(s, x)=\frac{1}{x}\frac{\sin(i\sqrt{s+\phi^2}x)}{3\frac{m_p/\rho_p}{V}\varepsilon_p[i\sqrt{\phi^2+s}\cos(i\sqrt{s+\phi^2})-\sin(i\sqrt{\phi^2+s})]+(s+\phi^2)i\sin(i\sqrt{s+\phi^2})} \text{ and}$$

$$Y_b(s)=\frac{1}{s+\phi^2}-\frac{1}{s+\phi^2}\frac{3\frac{m_p/\rho_p}{V}\varepsilon_p[(i\sqrt{s+\phi^2})\cos(i\sqrt{s+\phi^2})-\sin(i\sqrt{\phi^2+s})]}{3\frac{m_p/\rho_p}{V}\varepsilon_p[(i\sqrt{\phi^2+s})\cos(i\sqrt{s+\phi^2})-\sin(i\sqrt{s+\phi^2})]+(s+\phi^2)\sin(i\sqrt{s+\phi})} \tag{57}$$

Before inverse Laplace transform of $Y_p(x, s)$ and $Y_b(s)$, poles making the denominator of Eq. (57) as 0 should be determined. For this purpose, the following differential operator as matrix form can be defined for coupled differential equations to get eigenfunction $K_n(x)$ and D_n.

$$\underline{\underline{L}}=\begin{bmatrix}\frac{1}{x}\frac{d}{dx}\left(x\frac{d}{dx}\right)-\phi^2 & 0\\ -\frac{m_p/\rho_p}{V}\varepsilon_p\left(\frac{d}{dx}\right)_{x=1} & -\phi^2\end{bmatrix} \text{ and } \underline{K}_n=\begin{bmatrix}K_n\\ D_n\end{bmatrix} \tag{58}$$

After solving eigenvalue equation, $\underline{\underline{L}}\underline{K}_n=-\xi_n^2\underline{K}_n$ subject to boundary conditions such as $\left(\frac{dK_n(x)}{dx}\right)_{x=0}=0$ and $D_n=K_n(1)$, the eigenfunctions can be derived as $K_n(x)=\frac{\sin(\lambda_n x)}{x}$ and $D_n=\sin(\lambda_n)$. From Eq. (58), the following equation can be obtained to calculate the eigenvalues, λ_n, which are defined as $\lambda_n^2=\xi_n^2-\phi^2$.

$$3\frac{m_p/\rho_p}{V}\varepsilon_p(\lambda_n\cos\lambda_n-\sin\lambda_n)=\lambda_n^2\sin\lambda_n \tag{59}$$

The above transcendental equation can be solved numerically by Newton-Raphson method or graphically for necessary values of $\frac{m_p/\rho_p}{V}\varepsilon_p$, which is adjustable for operation of as slurry-type pho-

Table 5. Eigenvalues λ_n for various values of B=$\frac{m_p/\rho_p}{V}\varepsilon_p$ of coupled differential equations of batch-mode photocatalytic reactor in spherical coordinates

B	λ_1	λ_2	λ_3	λ_4	λ_5	λ_6	λ_7
1.73×10^{-5}	3.142	6.283	9.425	12.566	15.708	18.85	21.991
0.1	3.232	6.33	9.456	12.59	15.727	18.865	22.005
0.3	3.383	6.42	9.518	12.637	15.765	18.897	22.032
0.519	3.516	6.51	9.583	12.687	15.806	18.931	22.061
0.74	3.624	6.593	9.646	12.737	15.846	18.965	22.091
0.9	3.69	6.649	9.689	12.771	15.875	18.965	22.112
3	4.102	7.105	10.11	13.143	16.201	19.277	22.368
30	4.445	7.641	10.786	13.914	17.036	20.153	23.269

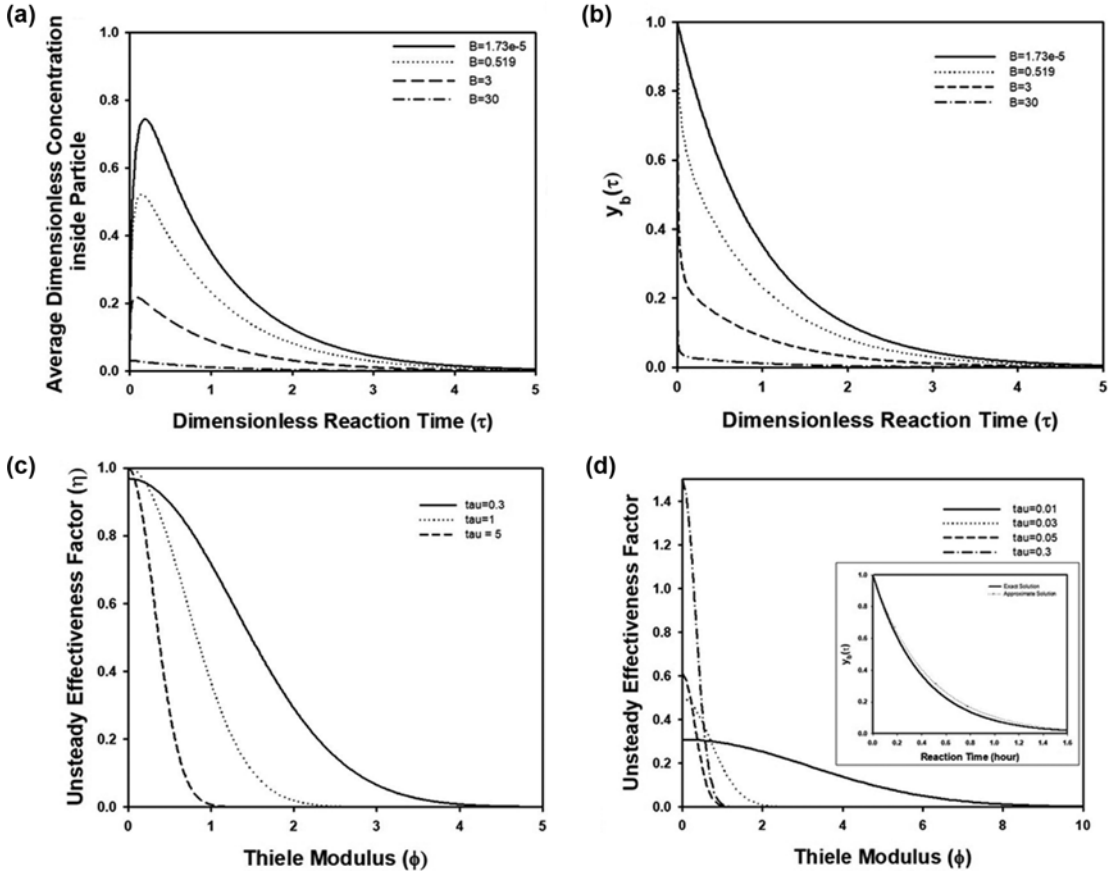

Fig. 9. (a) Change of average dimensionless concentration of reactant inside spherical porous particle in slurry-type batch reactor as a function of dimensionless reaction time (τ), when ϕ is fixed as 1.02. During calculation using exact solution, B=$\frac{m_p/\rho_p}{V}\varepsilon_p$ was adjusted as 1.73×10^{-5}, 0.519, 3, and 30. (b) Change of dimensionless bulk concentration, $y_b(\tau)$ in slurry-type batch photocatalytic reactor containing spherical porous photocatalytic particle as a function of dimensionless reaction time (τ), when ϕ was fixed as 1.02. During calculation using exact solution, B=$\frac{m_p/\rho_p}{V}\varepsilon_p$ was adjusted as 1.73×10^{-5}, 0.519, 3, and 30. (c) and (d) Unsteady effectiveness factor in spherical porous photocatalytic particle as a function of Thiele modulus (ϕ) calculated by exact and approximate mathematical solution, respectively. B=$\frac{m_p/\rho_p}{V}\varepsilon_p$ was adjusted as 1.73×10^{-5}. In inset figure of Fig. 8(d), $y_b(\tau)$ in spherical porous particle was compared using approximate and exact solutions.

tocatalytic batch reactor, as shown in Table 5.

By applying residue theorem, inverse Laplace transform can be carried out from the poles such as $\lambda_n = i\sqrt{s+\phi^2}$ or $s=-\phi^2$ to get the following exact solutions for spherical porous photocatalyst in

batch-mode reactor.

$$\bar{y}_p(\tau)=\frac{\exp(-\phi^2\tau)}{1+\frac{m_p/\rho_p}{V}\varepsilon_p}-\sum_{n=1}^{\infty}\frac{\exp\{-(\lambda_n^2+\phi)\tau\}}{\frac{3}{2}\left(\frac{m_p/\rho_p}{V}\varepsilon_p\right)^2+\frac{3}{2}\left(\frac{m_p/\rho_p}{V}\varepsilon_p\right)+\frac{\lambda_n^2}{6}} \quad (60)$$

$$y_b(\tau)=\frac{\exp(-\phi^2\tau)}{1+\frac{m_p/\rho_p}{V}\varepsilon_p}-\sum_{n=1}^{\infty}\frac{\frac{m_p/\rho_p}{V}\varepsilon_p\exp\{-(\lambda_n^2+\phi)\tau\}}{\frac{3}{2}\left(\frac{m_p/\rho_p}{V}\varepsilon_p\right)^2+\frac{3}{2}\left(\frac{m_p/\rho_p}{V}\varepsilon_p\right)+\frac{\lambda_n^2}{6}} \quad (61)$$

$\bar{y}_p(\tau)$ is the average concentration inside spherical porous particle, which is defined as $\bar{y}_p(\tau)=3\int_0^1 x^2 y_p(x,\tau)dx$ in spherical coordinate.

Since eigenvalues are not necessary for calculation, approximate solutions are convenient for prediction of concentration inside spherical porous particles or bulk transient concentration, though the mathematical solutions are composed of complicated functions. However, it is inevitable to accept the accuracy of calculation from the approximate solutions depending on the value of $B=\frac{m_p/\rho_p}{V}\varepsilon_p$. Thus, exact solutions in Eqs. (60) and (61) were adopted to investigate the effect of B on the concentrations, as displayed in Fig. 9. The maximum concentration of reactant inside spherical particles decreased drastically with increasing value of B, since concentrated suspension enhances the catalytic effect for the removal of reactant, as shown in Fig. 9(a). Similarly, transient bulk concentration also decreased with increasing value of B, since the mass flux from bulk fluid to particle surface as well as catalytic effect increased for removal of reactant, as displayed in Fig. 9(b).

In spherical porous particles, unsteady effectiveness factor, η defined as $\eta=\frac{\int_0^R 4\pi r^2 r_i dr}{\frac{4}{3}\pi R^2 r_{i,s}}$, is plotted in Fig. 9(c), based on the calculation results of exact mathematical solution in this section. Here, r_i and $r_{i,s}$ denote actual reaction rate inside particles and reaction rate assuming the particles are filled with reactant with surface concentration. The effectiveness factor in spherical porous particles is plotted in Fig. 9(c) for three different values of dimensionless reaction time, τ=0.3, 1, and 5. When reaction time was fixed, effectiveness factor decreased with increasing Thiele modulus (ϕ), indicating that increasing diffusion length caused diffusional resistance inside pores. As reaction time increased, this trend became more severe due to depletion of reactant and decreased reaction rate in first-order irreversible reaction. For comparison, the effectiveness factor calculated from approximate solution in previous section is shown in Fig. 9(d) from τ=0.01 to 0.3. When reaction time increased to τ=0.3, the effectiveness factor became larger than 1 for small value of Thiele modulus (ϕ), implying that it is difficult to apply the approximate solutions in the previous section for small value of ϕ. However, the approximate solution of $y_b(\tau)$ agreed well with the exact solution for small value of Thiele modulus (ϕ=0.0204), as compared in inset graph of Fig. 9(d).

Fig. 10 contains the effect of porosity (ε_p) on bulk concentration

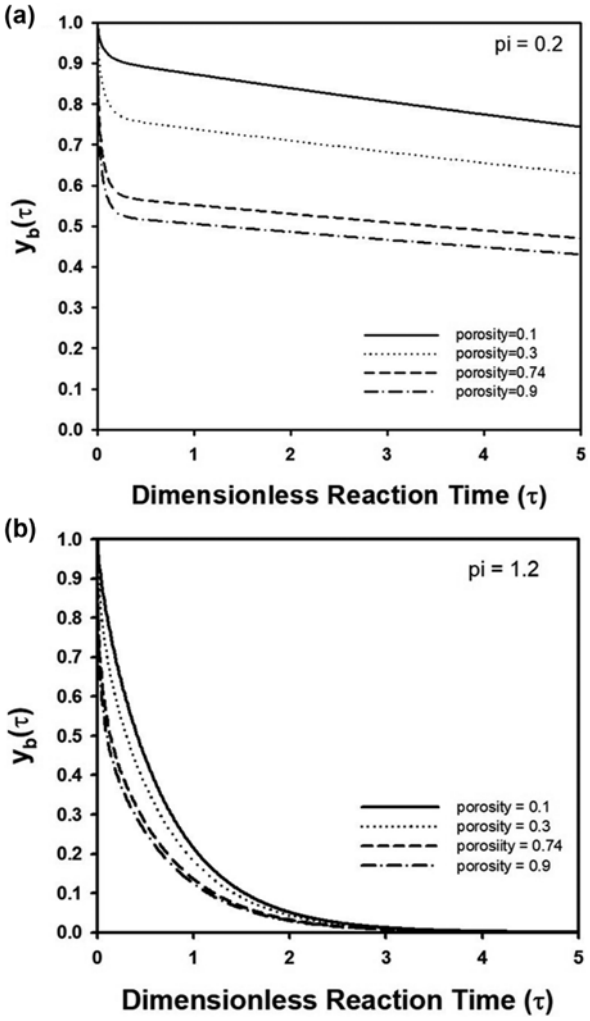

Fig. 10. (a) and (b) Change of dimensionless bulk concentration, $y_b(\tau)$ in slurry-type batch photocatalytic reactor containing spherical porous photocatalytic particle as a function of dimensionless reaction time (τ), when Thiele modulus, ϕ was fixed as 0.2 and 1.2, respectively. During calculation using exact solution, porosity (ε_p) was adjusted as 0.1, 0.3, 0.74, and 0.9. $\frac{m_p/\rho_p}{V}$ was fixed as 1.

inside reactor. Because the change of porosity affects the change of $B=\frac{m_p/\rho_p}{V}\varepsilon_p$, it is necessary to evaluate eigenvalues, λ_n, depending on the values of ε_p. For these calculations according to Eq. (59), $\frac{m_p/\rho_p}{V}$ was assumed as 1, while porosity was adjusted from 0.1 to 0.9, and the resulting values of eigenvalues are summarized in Table 5. When Thiele modulus was relatively small (ϕ=0.2), decreasing rate of bulk concentration increased drastically with increasing value of porosity, as shown in Fig. 10(a). In this case, particles with large porosity (ε_p=0.9) were much more effective than less porous particles (ε_p=0.1), since larger surface area for mass transfer to inner region of particles as well as more space for catalytic reaction inside particles can be provided from more porous particles. However, the dependency of bulk concentration became less important, when

Thiele modulus increased as relatively larger value (ϕ=1.2), as displayed in Fig. 10(b). Because highly porous aerogel particles can be synthesized as titania material, photocatalytic particles with high porosity can be potentially adopted in purification system [28].

5. Analytical Solutions of Transient Concentration Using Cylindrical Porous Photocatalytic Fibers in Slurry-type Batch Photocatalytic Reactor from Coupled Differential Equations

In addition to spherical porous catalytic particles, cylindrical particles were also examined to predict transient concentration in bulk phase and inside the particles from the coupled differential equations shown in Equations from (40) to (43). In cylindrical coordinates, the following coupled differential equation can be obtained after non-dimensionalization, assuming infinitely long cylindrical particles with negligible capping effect.

$$\frac{\partial y_p}{\partial \tau}=\frac{1}{x}\frac{\partial}{\partial x}\left(x\frac{\partial y_p}{\partial x}\right)-\phi^2 y_p \text{ (for cylinder)}$$

$$\text{subject to } y_p(x,\,o)=0,\ \left(\frac{\partial y_p}{\partial x}\right)_{x=0}=0 \text{ and } y_p(1,\,\tau)=y_b(1,\,\tau) \tag{62}$$

$$\frac{dy_b}{d\tau}=-2\frac{m_p/\rho_p}{V}\varepsilon_p\left(\frac{\partial y_p}{\partial x}\right)_{x=1}-\phi^2 y_b \text{ subject to } y_b(0)=1 \tag{63}$$

Assuming very large value of Biot number (Bi$\to\infty$), the following Laplace transform can be carried out.

$$\frac{1}{x}\frac{d}{dx}\left(x\frac{dY_p}{dx}\right)-(\phi^2+s)Y_p=0$$

$$\text{subject to } \left(\frac{dY_p}{dx}\right)_{x=0}=0 \text{ and } Y_p(1,\,s)=Y_b(s) \tag{64}$$

$$sY_b(s)-1=-2\frac{m_p/\rho_p}{V}\varepsilon_p\left(\frac{\partial y_p}{\partial x}\right)_{x=1}-\phi^2 Y_b(s) \tag{65}$$

The above equations can be solved in Laplace domain using undetermined coefficient A(s) and Bessel functions.

$$Y_p(x,\,s)=A(s)J_0(i\sqrt{s+\phi^2}\,x)$$

$$\text{and } Y_b(s)=\frac{1}{\phi^2+s}+2A(s)\frac{m_p/\rho_p}{V}\varepsilon_p(i\sqrt{\phi+s})J_1(i\sqrt{\phi^2+s}) \tag{66}$$

From the boundary condition shown in Eq. (64) at particle surface, A(s) can be determined to obtain $Y_p(x, s)$ and $Y_b(s)$ as the following form.

$$Y_p(s,\,x)=\frac{1}{s+\phi^2}\frac{i\sqrt{s+\phi^2}J_0(i\sqrt{s+\phi^2}\,x)}{2\frac{m_p/\rho_p}{V}\varepsilon_p J_1(i\sqrt{s+\phi^2})+i\sqrt{s+\phi^2}J_0(i\sqrt{s+\phi^2})} \text{ and}$$

$$Y_b(s)=\frac{1}{s+\phi^2} \tag{67}$$

$$-\frac{1}{s+\phi^2}\frac{2\frac{m_p/\rho_p}{V}\varepsilon_p(i\sqrt{s+\phi^2})J_1(i\sqrt{s+\phi^2})}{2\frac{m_p/\rho_p}{V}\varepsilon_p(i\sqrt{\phi^2+s})J_1(i\sqrt{s+\phi^2})-(s+\phi^2)J_0(i\sqrt{s+\phi})}$$

To apply residue theorem for inverse Laplace transform of $Y_p(s, x)$ and $Y_b(s)$, poles should be determined. To this end, the following operator for coupled differential equations is required to obtain eigenfunction $K_n(x)$ and D_n.

$$\underline{\underline{L}}=\begin{bmatrix}\frac{1}{x}\frac{d}{dx}\left(x\frac{d}{dx}\right)-\phi^2 & 0\\ -2\frac{m_p/\rho_p}{V}\varepsilon_p\left(\frac{d}{dx}\right)_{x=1} & -\phi^2\end{bmatrix} \text{ and } \underline{K}_n=\begin{bmatrix}K_n\\ D_n\end{bmatrix} \tag{68}$$

The eigenvalue equation, $\underline{\underline{L}}\underline{K}_n=-\xi_n^2\underline{K}_n$ can be solved assuming proper boundary conditions such as $\left(\frac{dK_n(x)}{dx}\right)_{x=0}=0$ and $D_n=K_n(1)$ to obtain the eigenfunctions as $K_n(x)=J_0(\lambda_n x)$ and $D_n=J_0(\lambda_n)$. The eigenvalues, λ_n, which are defined as $\lambda_n^2=\xi_n^2-\phi^2$ can be determined from Eq. (68) as the following equation.

$$2\frac{m_p/\rho_p}{V}\varepsilon_p J_1(\lambda_n)+\lambda_n J_0(\lambda_n)=0 \tag{69}$$

The above nonlinear algebraic equation can be solved graphically after fixing the value of $\frac{m_p/\rho_p}{V}\varepsilon_p$ as operating conditions of slurry-type photocatalytic batch reactor and plotting the left-hand side of the equation to find intersection points from horizontal axis. Table 5 contains a list of eigenvalues as an example.

For inverse Laplace transform of Eq. (67), the substitution, $\lambda_n=i\sqrt{s+\phi^2}$ can be adopted to determine the following transient concentrations.

$$\bar{y}_p(\tau)\cong\exp(-\phi^2\tau)-\sum_{n=1}^{\infty}\frac{\exp\{-(\lambda_n^2+\phi^2)\tau\}}{\left(\frac{m_p/\rho_p}{V}\varepsilon_p\right)^2+\frac{m_p/\rho_p}{V}\varepsilon_p+\frac{\lambda_n^2}{4}} \tag{70}$$

$$y_b(\tau)=\frac{\exp(-\phi^2\tau)}{1+\frac{m_p/\rho_p}{V}\varepsilon_p}+\sum_{n=1}^{\infty}\frac{\frac{m_p/\rho_p}{V}\varepsilon_p\exp\{-(\lambda_n^2+\phi^2)\tau\}}{\left(\frac{m_p/\rho_p}{V}\varepsilon_p\right)^2+\frac{m_p/\rho_p}{V}\varepsilon_p+\frac{\lambda_n^2}{4}} \tag{71}$$

During derivation of Eq. (70), A slurry-type photocatalytic reactor using diluted suspension with small value of $\frac{m_p/\rho_p}{V}\varepsilon_p$ was assumed to obtain an approximate solution. The average concentration inside

Table 6. Eigenvalues λ_n for various values of B=$\frac{m_p/\rho_p}{V}\varepsilon_p$ of coupled differential equations of batch-mode photocatalytic reactor in cylindrical coordinates

B	λ_1	λ_2	λ_3	λ_4	λ_5	λ_6	λ_7
1.73×10^{-5}	2.405	5.52	8.654	11.792	14.931	18.071	21.212
0.173	2.537	5.582	8.693	11.821	14.954	18.09	21.228
0.519	2.744	5.697	8.771	11.878	15	18.128	21.26
3	3.353	6.248	9.215	12.239	15.3	18.384	21.482
30	3.769	6.902	10.009	13.11	16.209	19.307	22.405

particles, $\bar{y}_p(\tau)$ was obtained from the definition of average concentration in cylindrical coordinates, $\bar{y}_p(\tau)=2\int_0^1 x y_p(x,\ \tau)dx$.

Table 6 contains the eigenvalues, in which $\frac{m_p/\rho_p}{V}\varepsilon_p$ was adjusted as 1.73×10^{-5}, which is necessary value to calculate transient concentrations of reactant in diluted suspension as a function of reaction time. When the value of $\frac{m_p/\rho_p}{V}\varepsilon_p$ was smaller than 1.73×10^{-2}, the eigenvalues were maintained as similar values summarized in Table 6. Using these eigenvalues and the mathematical solution in Eq. (71), $y_b(\tau)$ was plotted assuming that physicochemical properties of cylindrical porous titania microfibers can be found from Table 4, except variable Thiele modulus ϕ. In Fig. 11(a), the change of bulk concentration, $y_b(\tau)$ is plotted as a function of reaction time for three values of Thiele modulus such as ϕ=0.0102, 0.0204, and 0.0408. As Thiele modulus increased, the rate of photocatalytic decomposition reaction increased, causing rapid reduction of reactant concentration in bulk fluid, as shown in Fig. 11(a). Fig. 11(b) displays the change of average dimensionless concentration of reactant inside cylindrical porous particles, $\bar{y}_p(\tau)$, which was calculated from the approximate solution in Eq. (70), as a function of reaction time for ϕ=0.0102, 0.0204, and 0.0408. As Thiele modulus decreased, increasing rate of $\bar{y}_p(\tau)$ to its maximum value became slower due to decreased reaction rate for depletion of reactant. On the contrary, maximum value of $\bar{y}_p(\tau)$ decreased with increasing value of Thiele modulus, as shown in Fig. 11(b). Regardless of the value of the Thiele modulus, the concentration of reac-

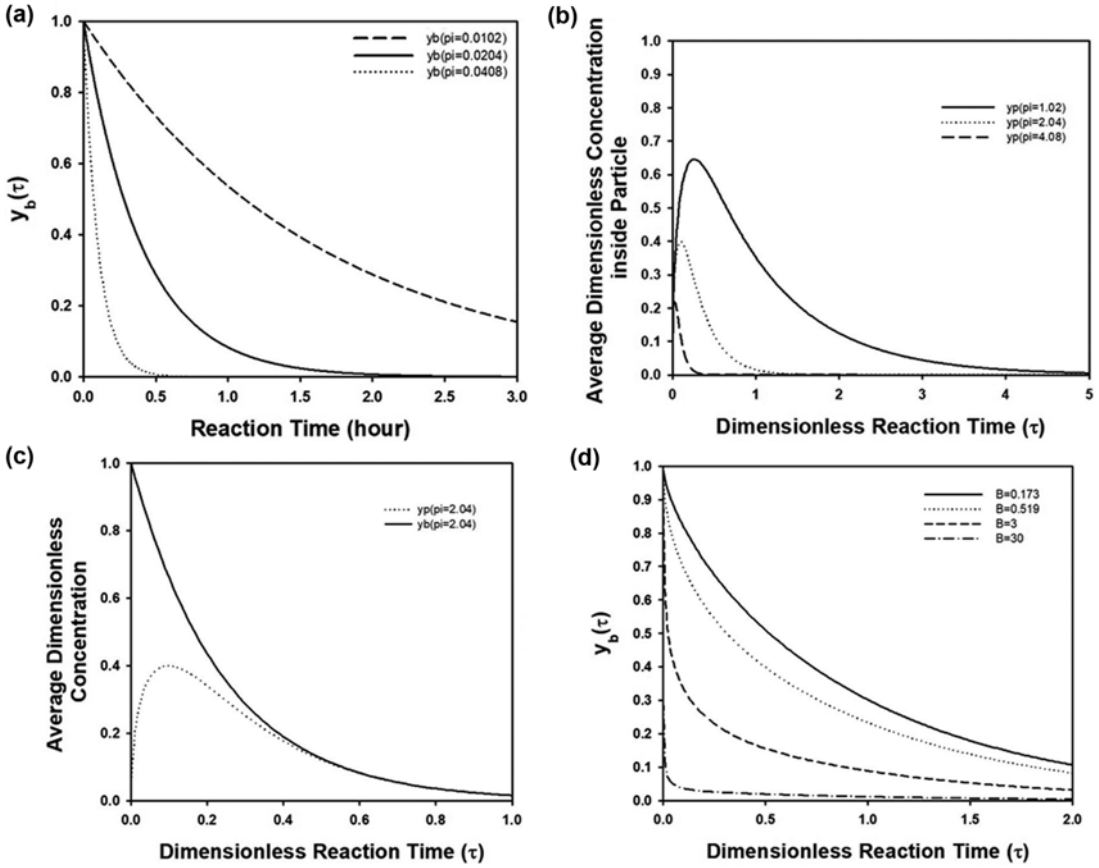

Fig. 11. (a) Change of bulk concentration $y_b(\tau)$ in slurry-type batch reactor containing cylindrical porous photocatalytic particles as a function of reaction time. ϕ was adjusted as 0.0102, 0.0204, and 0.0408, respectively. B=$\frac{m_p/\rho_p}{V}\varepsilon_p$ was assumed as small value like 1.73×10^{-5} in diluted suspension. (b) Change of average concentration of reactant inside cylindrical porous particles as a function of dimensionless reaction time. ϕ was adjusted as 1.02, 2.04, and 4.08, respectively. B=$\frac{m_p/\rho_p}{V}\varepsilon_p$ was assumed as small value like 1.73×10^{-5} in diluted suspension. (c) Change of average dimensionless concentration of reactant inside cylindrical porous particle as a function of dimensionless reaction time (dotted line). For comparison, change of bulk concentration, $y_b(\tau)$ is also plotted in the same graph as solid line. ϕ was assumed as 2.04 and B=$\frac{m_p/\rho_p}{V}\varepsilon_p$ was fixed as 1.73×10^{-5} in diluted suspension. (d) Change of bulk concentration $y_b(\tau)$ in slurry-type batch reactor containing cylindrical porous photocatalytic particles as a function of reaction time. B=$\frac{m_p/\rho_p}{V}\varepsilon_p$ was adjusted as 0.173, 0.519, 3, and 30, respectively, while ϕ was fixed as 1.02.

tant decreased to zero after the reaction progressed sufficiently. For comparison, the transient bulk concentration, $y_b(\tau)$ is plotted with $\bar{y}_p(\tau)$ in Fig. 11(c). In the initial stage of reaction, mass transfer between bulk phase to particles occurred due to the concentration difference between fluid and solid phases. However, reactant concentration inside particles decreased after its maximum value, implying that depletion rate of reactant became dominant over inward flux of reactant material to the particles.

In addition to Thiele modulus, the bulk concentration of reactant during photocatalytic decomposition reaction can be adjusted by changing the value of $\frac{m_p/\rho_p}{V}\varepsilon_p$ (noted as B inside the graph), as displayed in Fig. 11(d). Since the bulk concentration shown in Eq. (71) is an exact solution, it is applicable to any value of $\frac{m_p/\rho_p}{V}\varepsilon_p$, if eigenvalues λ_n are known, as shown in Table 6. By increasing the suspended amount of particulate materials inside batch-mode reactor as increasing value of $\frac{m_p/\rho_p}{V}\varepsilon_p$, the adsorbed amount of reactant on the surface of the catalytic materials will be increased, causing faster decrease of the bulk concentration of reactant under fixed value of Thiele modulus ϕ=1.02 during light illumination time. This affected the concentration decrease in the early stage of reaction, as displayed in Fig. 11(d).

The approximate solution shown in Eq. (70) is applicable to diluted suspension ($\frac{m_p/\rho_p}{V}\varepsilon_p \ll 1$). For very concentrated suspension, another approximate solution can be obtained as the following form, which can be applied to another limiting case, $\frac{m_p/\rho_p}{V}\varepsilon_p \gg 1$.

$$\bar{y}_p(\tau) \cong \frac{\exp(-\phi^2\tau)}{\frac{m_p/\rho_p}{V}\varepsilon_p} - \sum_{n=1}^{\infty} \frac{\exp\{-(\lambda_n^2+\phi^2)\tau\}}{\left(\frac{m_p/\rho_p}{V}\varepsilon_p\right)^2 + \frac{m_p/\rho_p}{V}\varepsilon_p + \frac{\lambda_n^2}{4}} \quad (72)$$

Since the above equation was obtained during residue calculation by applying $\frac{m_p/\rho_p}{V}\varepsilon_p >> 1$, it was applied to predict the transient average concentration inside particles when $B=\frac{m_p/\rho_p}{V}\varepsilon_p$ was fixed as 30, as shown in the graph of Fig. 12(a). For three different value of Thiele modulus ϕ=0.204, 1.02, and 2.04, the maximum average concentration was calculated as quite small values, since concentrated suspension was used to remove contaminant (reactant) by first order irreversible reaction.

By matching the approximate solutions in Eqs. (70) and (72), an exact solution inside porous cylindrical particle can be deduced in the following manner, which can be confirmed by Laplace transform yielding Eq. (67).

$$\bar{y}_p(\tau) = \frac{\exp(-\phi^2\tau)}{1+\frac{m_p/\rho_p}{V}\varepsilon_p} - \sum_{n=1}^{\infty} \frac{\exp\{-(\lambda_n^2+\phi^2)\tau\}}{\left(\frac{m_p/\rho_p}{V}\varepsilon_p\right)^2 + \frac{m_p/\rho_p}{V}\varepsilon_p + \frac{\lambda_n^2}{4}} \quad (73)$$

Fig. 12(b) contains unsteady effectiveness factor, $\eta = \frac{\int_0^R 2\pi r L r_i dr}{\pi R^2 r_{i,s}}$,

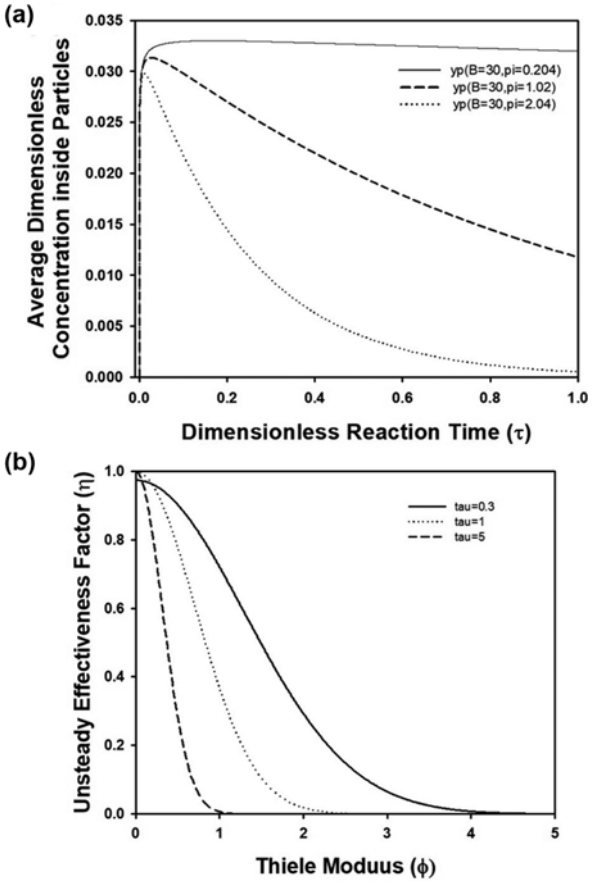

Fig. 12. (a) Change of average dimensionless concentration of reactant inside cylindrical porous particle as a function of dimensionless reaction time. ϕ was adjusted as 0.204, 1.02, and 2.04, respectively. $B=\frac{m_p/\rho_p}{V}\varepsilon_p$ was assumed as large value like 30 in concentrated suspension. (b) Unsteady effectiveness factor in cylindrical porous photocatalytic particle as a function of Thiele modulus (ϕ). $B=\frac{m_p/\rho_p}{V}\varepsilon_p$ was assumed as small value like 1.73×10^{-5} in diluted suspension.

which is defined as the ratio of actual reaction rate inside porous cylindrical particles to the rate of reaction when reactant concentration is maintained as surface concentration. Here, r_i and $r_{i,s}$ denote the reaction rate of reactant inside particles or particle surface, respectively. As shown in Fig. 12(b), the effectiveness factor decreased with increasing value of Thiele modulus (ϕ), implying that diffusion resistance inside porous particles became significant. With increasing reaction time, the decreasing rate of effectiveness factor became faster, indicating that contribution of the reaction became less important, since reaction rate is proportional to the concentration of reactant concentration in first-order reaction, which decreased with increasing reaction time.

6. Analytical Solutions of Transient Concentration Using Slab-type Porous Photocatalytic Fibers in Slurry-type Batch Photocatalytic Reactor from Coupled Differential Equations

In addition to spherical or cylindrical porous particles, analytical solutions of transient concentration were obtained in rectangu-

lar-shaped particles as the final topic in this article. In slab-type porous catalytic particles suspended inside batch photocatalytic reactor, the following governing equations can be derived from material balance as coupled differential equation.

$$\frac{\partial y_p}{\partial \tau}=\frac{\partial^2 y_p}{\partial x^2}-\phi^2 y_p \text{ (for slab)}$$

$$\text{subject to } y_p(x,\,o)=0,\left(\frac{\partial y_p}{\partial x}\right)_{x=0}=0 \text{ and } y_p(1,\,\tau)=y_b(\tau) \tag{74}$$

$$\frac{dy_b}{d\tau}=-\frac{m_p/\rho_p}{V}\varepsilon_p\left(\frac{\partial y_p}{\partial x}\right)_{x=1}-\phi^2 y_b \text{ subject to } y_b(0)=1 \tag{75}$$

After Laplace transform of the above equations, concentration inside slab-type particles and bulk phase can be obtained as the following forms in Laplace domain.

$$Y_p(s,\,x)=\frac{\cos(i\sqrt{s+\phi^2}\,x)}{-\frac{m_p/\rho_p}{V}\varepsilon_p i\sqrt{s+\phi^2}\sin(i\sqrt{s+\phi^2})+(s+\phi^2)\cos(i\sqrt{s+\phi^2})} \text{ and}$$

$$Y_b(s)=\frac{1}{s+\phi^2} \tag{76}$$
$$+\frac{1}{s+\phi^2}\frac{\frac{m_p/\rho_p}{V}\varepsilon_p(i\sqrt{s+\phi^2})\sin(i\sqrt{s+\phi^2})}{-\frac{m_p/\rho_p}{V}\varepsilon_p(i\sqrt{\phi^2+s})\sin(i\sqrt{s+\phi^2})+(s+\phi^2)\cos(i\sqrt{s+\phi})}$$

For inverse Laplace transform of the above equations by residue theorem, the following eigenvalue problems can be defined to obtain poles.

$$\underline{\underline{L}}=\begin{bmatrix}\frac{d^2}{dx^2}-\phi^2 & 0\\ -\frac{m_p/\rho_p}{V}\varepsilon_p\left(\frac{d}{dx}\right)_{x=1} & -\phi^2\end{bmatrix} \text{ and } \underline{K}_n=\begin{bmatrix}K_n\\ D_n\end{bmatrix} \tag{77}$$

The eigenfunctions satisfy the eigenvalue equation, $\underline{\underline{L}}\underline{K}_n=-\xi_n^2\underline{K}_n$ can be found as $K_n(x)=\cos(\lambda_n x)$ and $D_n=\cos(\lambda_n)$ by applying boundary conditions such as $\left(\frac{dK_n(x)}{dx}\right)_{x=0}=0$ and $D_n=K_n(1)$. Thus, eigenvalues, λ_n, defined as $\lambda_n^2=\xi_n^2-\phi^2$ can be found by solving the following nonlinear equation.

$$\frac{m_p/\rho_p}{V}\varepsilon_p\sin(\lambda_n)+\lambda_n\cos(\lambda_n)=0 \tag{78}$$

In Table 7, the value of λ_n for $B=\frac{m_p/\rho_p}{V}\varepsilon_p$ is summarized, since eigenvalues are necessary to predict transient behavior inside batch-type photocatalytic reactor. After inverse Laplace transform, the following mathematical solutions can be obtained for slab-type photocatalytic particles.

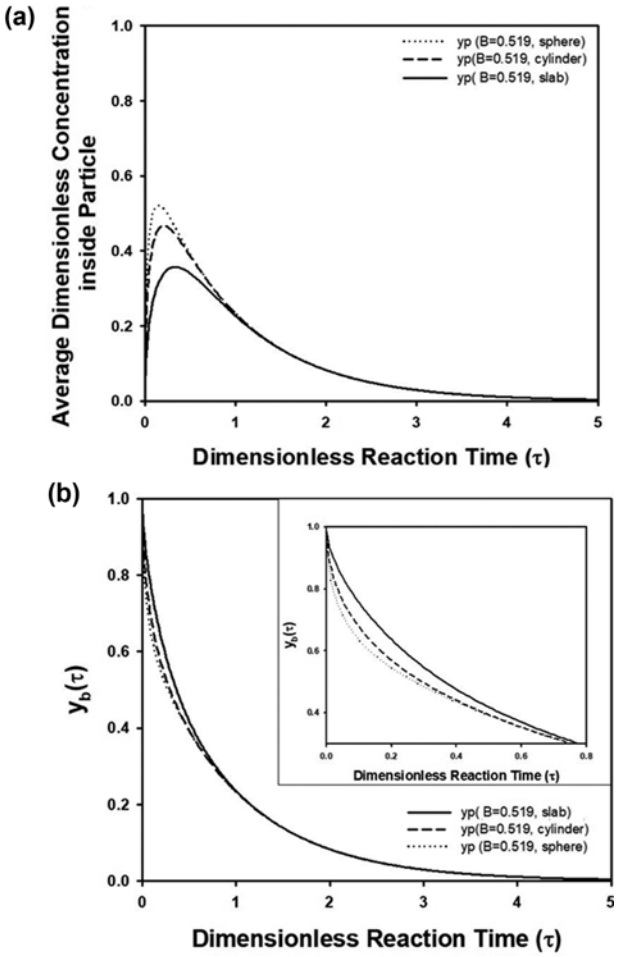

Fig. 13. (a) Change of average dimensionless concentration of reactant inside porous particle with spherical, cylindrical, and slab-type morphologies as a function of dimensionless reaction time. ϕ and $B=\frac{m_p/\rho_p}{V}\varepsilon_p$ were fixed as 1.02 and 0.519, respectively, for three types of particles. (b) Change of dimensionless bulk concentration of reactant in batch-type photocatalytic reactor containing porous particle with spherical, cylindrical, and slab-type morphologies as a function of dimensionless reaction time. ϕ and $B=\frac{m_p/\rho_p}{V}\varepsilon_p$ were fixed as 1.02 and 0.519, respectively, for three types of particles. Inset figure contains the magnified graph for initial stage of reaction.

$$\bar{y}_p(\tau)\cong\frac{\exp(-\phi^2\tau)}{1+\frac{m_p/\rho_p}{V}\varepsilon_p}-\sum_{n=1}^{\infty}\frac{\exp\{-(\lambda_n^2+\phi^2)\tau\}}{\frac{1}{2}\left(\frac{m_p/\rho_p}{V}\varepsilon_p\right)^2+\frac{1}{2}\frac{m_p/\rho_p}{V}\varepsilon_p+\frac{\lambda_n^2}{2}} \tag{79}$$

Table 7. Eigenvalues λ_n for various values of $B=\frac{m_p/\rho_p}{V}\varepsilon_p$ of coupled differential equations of batch-mode photocatalytic reactor in cartesian coordinates

B	λ_1	λ_2	λ_3	λ_4	λ_5	λ_6	λ_7
1.73×10^{-5}	1.571	4.712	7.854	10.996	14.137	17.279	20.42
0.519	1.845	4.82	7.919	11.043	14.174	17.309	20.446

$$y_b(\tau)=\frac{\exp(-\phi^2\tau)}{1+\frac{m_p/\rho_p}{V}\varepsilon_p}+\sum_{n=1}^{\infty}\frac{\frac{m_p/\rho_p}{V}\varepsilon_p\exp\{-(\lambda_n^2+\phi^2)\tau\}}{\frac{1}{2}\left(\frac{m_p/\rho_p}{V}\varepsilon_p\right)^2+\frac{1}{2}\frac{m_p/\rho_p}{V}\varepsilon_p+\frac{\lambda_n^2}{4}} \quad (80)$$

For comparison, the average concentration of reactant inside porous catalytic particles with spherical, cylindrical, and slab-type morphologies is plotted in Fig. 13(a). The overall behavior of $\overline{y}_p(\tau)$ was predicted as highest concentration inside spherical particle, whereas the lowest concentration was calculated inside slab-type particle. Since diffusional flux from bulk to particle surface is proportional to surface-to-volume ratio, the largest inward transport of reactant can be expected in a spherical particle, increasing the value of reactant concentration, compared to other types of particles, as shown in Fig. 13(a). On the contrary, rapid decreasing rate of bulk concentration, $y_b(\tau)$ in batch reactor containing spherical porous photocatalytic particles was observed from mathematical calculation, compared to other types of particles as shown in Fig. 13(b), since diffusion flux from bulk to surface of spherical particles is faster than that of catalytic particles with different morphology. Thus, it can be concluded that spherical porous photocatalytic particles are the most advantageous for fast removal of reactant in batch reactor, although the reaction order in bulk phase is the same for all kinds of particles.

7. Analytical Solutions of Transient Concentration using Slab-type Porous Photocatalytic Fibers in Slurry-type CSTR Photocatalytic Reactor from Coupled Differential Equations

Since continuous operation of water treatment system is available, a CSTR reactor can be more practical compared to batch-mode photocatalytic reactor. Fig. 14(a) contains a schematic figure of photocatalytic CSTR reactor. In the outlet stream, a filter for excluding photocatalytic particles was assumed, whereas pure contaminated feed stream was supposed without particulate materials. Photocatalytic particles were considered as suspended only inside the eactor. Due to inlet and outlet flow surrounding CSTR reactor, material balance equations become more complicated than the results from batch reactor, in the following manner. For convenience, slab-type particles were assumed as photocatalytic material during derivation of the governing equations.

$$\varepsilon_p\frac{\partial c_p}{\partial t}=D_e\frac{\partial^2 c_p}{\partial r^2}-kc_p$$

$$\text{subject to } c_p(r,o)=0,\ \left(\frac{\partial c_p}{\partial r}\right)_{r=0}=0 \text{ and } c_p(R,t)=c_b(t) \quad (81)$$

$$\frac{dc_b}{dt}=-\frac{1}{R}\frac{m_p/\rho_p}{V}D_e\left(\frac{\partial c_p}{\partial r}\right)_{r=R}+\frac{F}{V}c_0-\left(\frac{F}{V}+k\right)c_b \text{ subject to } c_b(0)=c_0 \quad (82)$$

Here, V and F are reactor volume and flow rate of reactant, respectively. V/F is retention time of reactant inside CSTR reactor, which is also called as space time, τ_s. After non-dimensionalization, the following coupled differential equations can be derived.

$$\frac{\partial y_p}{\partial\tau}=\frac{\partial^2 y_p}{\partial x^2}-\phi^2 y_p \text{ (for slab)}$$

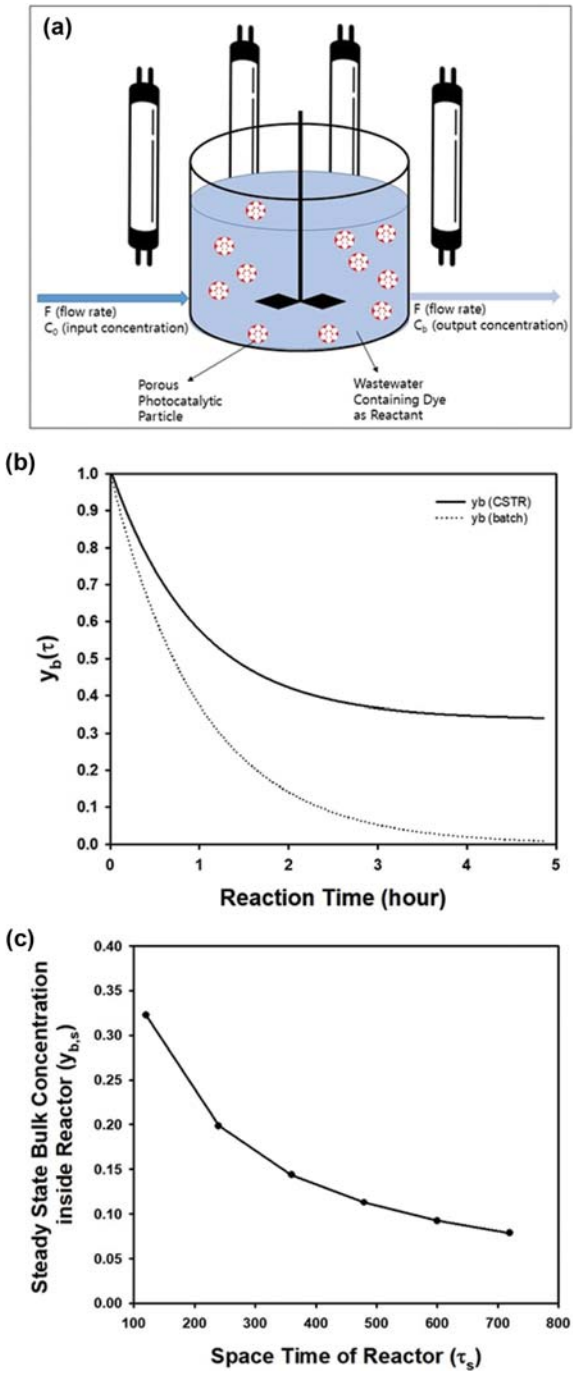

Fig. 14. (a) Schematic figure of photocatalytic CSTR reactor containing porous catalytic particles. (b) Change of dimensionless bulk concentration of reactant in slurry-type photocatalytic reactor (CSTR) containing slab-type porous particle as a function of dimensionless reaction time. For comparison, the bulk concentration in batch reactor under the same reaction conditions is also plotted in the same graph as dotted line. For calculation, ϕ and $B=\frac{m_p/\rho_p}{V}\varepsilon_p$ were fixed as 0.0126 and 1.73×10^{-5}, respectively, while space time was fixed as 120 minutes. (c) Change of steady-state concentration, $y_{b,s}$ in photocatalytic CSTR reactor containing slab-type porous particles as a function of space time in photocatalytic CSTR reactor.

$$\text{subject to } y_p(x,\,o)=0,\ \left(\frac{\partial y_p}{\partial x}\right)_{x=0}=0 \ \&\ y_p(1,\,\tau)=y_b(\tau) \tag{83}$$

$$\frac{dy_b}{d\tau}=-\frac{m_p/\rho_p}{V}\varepsilon_p\left(\frac{\partial y_p}{\partial x}\right)_{x=1}+\frac{R^2\varepsilon_p}{\tau_s D_e} -\left(\frac{R^2\varepsilon_p}{\tau D_e}-\phi^2\right)y_b \text{ subject to } y_b(0)=1 \tag{84}$$

Sine Eq. (84) is nonhomogeneous, it is convenient to separate the bulk concentration as the summation of transient and constant value, $y_b(\tau)=y_b^t(\tau)+y_{b,s}$. If the following ordinary differential equation is set for $y_b^t(\tau)$, it is easy to determine $y_{b,s}$ as $1/(1+k\tau_s)$.

$$\frac{dy_b^t}{d\tau}=-\frac{m_p/\rho_p}{V}\varepsilon_p\left(\frac{\partial y_p}{\partial x}\right)_{x=1} -\left(\frac{R^2\varepsilon_p}{\tau D_e}-\phi^2\right)y_b^t \text{ subject to } y_b^t(0)=\frac{k\tau_s}{1+k\tau_s} \tag{85}$$

For convenience, the boundary condition at x=1 in Eq. (83) can be changed as $y_p(1,\,\tau)=y_b^t(\tau)+y_{b,s}$ After Laplace transform, the above coupled differential equations can be solved as the following results for bulk concentration in Laplace domain.

$$Y_b^t(s)=\frac{k\tau_s}{1+k\tau_s}\frac{1}{s+\frac{R^2\varepsilon_p}{\tau_s D_e}+\phi^2} +\frac{1}{s}\frac{k\tau_s}{(1+k\tau_s)^2}\frac{\frac{m_p/\rho_p}{V}\varepsilon_p(i\sqrt{s+\phi^2})\sin(i\sqrt{s+\phi^2})}{-\frac{k\tau_s}{1+k\tau_s}\frac{m_p/\rho_p}{V}\varepsilon_p(i\sqrt{\phi^2+s})\sin(i\sqrt{s+\phi^2})+\left(s+\frac{R^2\varepsilon_p}{\tau_s D_e}+\phi^2\right)\cos(i\sqrt{s+\phi})} +\frac{\left(\frac{k\tau_s}{1+k\tau_s}\right)^2}{s+\frac{R^2\varepsilon_p}{\tau_s D_e}+\phi^2-\frac{k\tau_s}{1+k\tau_s}\frac{m_p/\rho_p}{V}\varepsilon_p(i\sqrt{\phi^2+s})\sin(i\sqrt{s+\phi^2})+\left(s+\frac{R^2\varepsilon_p}{\tau_s D_e}+\phi^2\right)\cos(i\sqrt{s+\phi})} \frac{m_p/\rho_p}{V}\varepsilon_p(i\sqrt{s+\phi^2})\sin(i\sqrt{s+\phi^2}) \tag{86}$$

$$\text{and } Y_{b,s}=\frac{1}{(1+k\tau_s)s}$$

To find the inverse transform of $Y_b(s)$ by residue theorem, poles such as $s_n=-\lambda_n^2-\phi^2$ can be found by estimating the roots satisfying the following transcendental equation, which is the same for $\tau_s\to\infty$.

$$\frac{k\tau_s}{1+k\tau_s}\frac{m_p/\rho_p}{V}\varepsilon_p\lambda_n\sin(\lambda_n)+\left(\lambda_n^2-\frac{R^{2\varepsilon}\varepsilon_p}{\tau_s D_e}\right)\cos(\lambda_n)=0 \tag{87}$$

Table 8 contains the numerical values of poles for various values of space time, τ_s, when $B=\frac{m_p/\rho_p}{V}\varepsilon_p$ was fixed as 1.73×10^{-5} in diluted suspension. When space time changed from 120 to 720 minutes, the value of λ_1 changed slightly, whereas other poles remained as almost the same values.

By applying residue theorem from poles such as $s_n=-\lambda_n^2-\phi^2$ and $s=-\phi^2-\frac{R^{2\varepsilon}\varepsilon_p}{\tau_s D_e}$, the bulk concentration inside CSTR reactor can be predicted as the following complicated equation after convolution integration.

$$y_b(\tau)=\frac{1}{1+k\tau_s}+\sum_{n=1}^{\infty}\frac{k\tau_s}{\frac{R^2\varepsilon_p}{\tau_s D_e}-\lambda_n^2}f_n(\tau)-\sum_{n=1}^{\infty}\frac{1}{\lambda_n^2+\phi^2}f_n(\tau)+\sum_{n=1}^{\infty}\frac{1}{\lambda_n^2+\phi^2}f_n(0)$$

$$f_n(\tau)=\frac{\frac{1}{1+k\tau_s}\frac{m_p/\rho_p}{V}\varepsilon_p\exp[-(\lambda_n^2+\phi^2)\tau]}{\frac{\frac{m_p/\rho_p}{V}\varepsilon_p}{\frac{R^2\varepsilon_p}{\tau_s D_e}-\lambda_n^2}+\frac{1}{2\lambda_n^2}\frac{1+k\tau_s}{k\tau_s}\left(\frac{R^2\varepsilon_p}{\tau_s D_e}-\lambda_n^2\right)+\frac{1}{\lambda_n^2}\frac{m_p/\rho_p}{V}\varepsilon_p +\frac{1}{2}\frac{k\tau_s}{1+k\tau_s}\left(\frac{m_p/\rho_p}{V}\varepsilon_p\right)^2\frac{1}{\frac{R^2\varepsilon_p}{\tau_s D_e}-\lambda_n^2}} \tag{88}$$

Fig. 14(b) contains the change of bulk concentration of reactant, $y_b(\tau)$ in CSTR reactor (solid line), when space time τ_s was fixed as 120 minutes, while B and ϕ were fixed as 1.73×10^{-5} and 0.0126, respectively. Under the same values of B and ϕ, change of bulk concentration of reactant in batch-mode reactor is also plotted as dotted line in the same graph. Since fresh wastewater contained dye molecules with constant concentration toward CSTR reactor, complete removal of reactant was not possible, whereas reaction conversion reached to almost 100% in batch-mode reactor after 5 hours. Since only limited amount of reactant should be treated in a batch reactor, complete removal of toxic dyes was possible, based on the prediction results of coupled differential equations.

To increase reaction conversion from CSTR reactor, three methods can be adopted. As the first way, photocatalytic particles can be replaced with other materials having larger photocatalytic activity. Secondly, the amount of photocatalytic materials can be increased to enhance the decomposition rate of reactant. Finally, space time can be also extended by decreasing feed rate of reactant, which is equal value with drain rate of treated water flow from reactor. In this article, the third way was briefly studied by investigating the effect of space time on steady state value of bulk concentration in CSTR reactor. In the limit of infinite dimensionless reaction time ($\tau\to\infty$) in Eq. (88), the steady-state bulk concentration, $y_{b,s}$, can be determined from the following equation.

$$y_{b,s}=\frac{1}{1+k\tau_s}+\sum_{n=1}^{\infty}\frac{1}{\lambda_n^2+\phi^2}f_n(0) \tag{89}$$

Table 8. Poles λ_n for various values of space time τ_s of coupled differential equations of CSTR photocatalytic reactor in cartesian coordinates

τ_s	$k\tau_s$	λ_1	λ_2	λ_3	λ_4	λ_5	λ_6	λ_7
120 min	1.92	0.00289	1.571	4.712	7.854	10.996	14.137	17.279
240 min	3.84	0.002	1.571	4.712	7.854	10.996	14.137	17.279
360 min	5.76	0.0017	1.571	4.712	7.854	10.996	14.137	17.279
480 min	7.68	0.0014	1.571	4.712	7.854	10.996	14.137	17.279
600 min	9.6	0.00129	1.571	4.712	7.854	10.996	14.137	17.279
720 min	11.52	0.00121	1.571	4.712	7.854	10.996	14.137	17.279

The predicted value of steady-state bulk concentration, $y_{b,s}$ inside CSTR reactor in Fig. 14(b) was about 0.33, which coincided well with the calculated value from Eq. (89).

Fig. 14(c) contains the change of $y_{b,s}$, as a function space time τ_s. By increasing space time from 120 to 720 minutes, the final steady state concentration of reactant could be reduced from 33 to 7.9% with respect to concentration of reactant in inlet flow. However, the start-up period can be prolonged to reach the steady-state concentration, when space time is increased to several hours.

For more complicated shapes such as spherical or cylindrical porous particles, the modeling and calculation for CSTR reactors are underway for future works. The comparison with the results from slab-type photocatalytic particles will be treated in the next paper, including other types of reactors such as packed bed or recycle reactors.

As remaining issues, our solutions obtained by considering Biot number for different geometries can be compared with numerical solutions to investigate the origin of discrepancies. After foundation of the measurement method of Biot number, experimental results can be also compared with the analytic and numerical solutions to inspect the theoretical treatment of reaction-diffusion equation. Numerical solutions of the coupled differential equations in this study can be also compared with our approximate solutions for various parameters to establish the reliable conditions of the approximate solutions. Upgraded version of analytical or approximate solutions can be also found for more complicated systems with time-dependent rate constant for reflection of catalyst deactivation. All these topics are underway for future researches.

CONCLUSIONS

Unsteady reaction-diffusion equation with irreversible first order reaction was solved by eigenfunction expansion method for spherical porous catalytic particles subject to convective boundary condition on particle surface, assuming exponentially decaying bulk concentration. The mathematical solutions are applicable to any arbitrary values of the Biot number, which can be changed according to various situations in experimental systems. The concentration profile as well as average concentration inside the spherical porous particles could be obtained as a function of position inside particle or reaction time, respectively, by adjusting several parameters such as Thiele modulus and Biot number. Laplace transform could be also applied to solve the reaction-diffusion equation in cylindrical coordinates to predict the concentration profile or average concentration inside infinitely long cylindrical porous catalytic particles. Since the solution was also applicable to any value of Biot number, the general solution was more advantageous compared to our previous researches. With increasing value of Biot number, the concentration inside cylindrical particles increased due to the decrease of external mass transfer resistance, which enhanced mass transfer from bulk fluid phase to the particles. Similar results could be obtained from mathematical solution of slab-type porous catalytic particles subject to exponentially decaying bulk concentration of reactant, which was obtained by eigenfunction expansion method. As an application, the cylindrical porous particles were synthesized as macroporous titania fibers, and methylene blue was removed from aqueous medium by photocatalytic decomposition mechanism. The measured values of reactant concentration in water were compared with average concentration inside the cylindrical particles and by assuming different values of Biot number and porosity to tortuosity ratio of the particles.

In addition to reactant concentration inside particles, the transient behavior of bulk concentration could be also calculated by solving coupled differential equations, which are adequate to slurry-type photocatalytic reactor operated as batch mode. Laplace transform could be applied to approximate solutions of bulk concentration in batch reactor containing spherical, cylindrical, or slab-type porous catalytic particles. Factors affecting transient bulk concentration were also elucidated by adjusting reaction parameters such as Thiele modulus and the concentration of catalytic particles or volume of reactor. Reactant concentration inside catalytic particles as well as unsteady effectiveness factor could be also predicted as approximate manner during inverse Laplace transform to compare the transient behavior with change of bulk concentration. The reactant in bulk phase and inside the catalytic particles could be removed effectively by increasing Thiele modulus and the concentration of catalytic particles in batch-mode photocatalytic reactor. Since surface-to-volume ratio of spherical porous particle is the largest among three kinds of particle morphologies in this study, the most rapid reduction rate of bulk concentration of reactant was observed from the mathematical solutions under the same reaction conditions, due to enhanced diffusional flux the of reactant to the particle surface. Effect of porosity of photocatalytic particles on removal of reactant in batch photocatalytic reactor was also studied, indicating that removal rate became more faster with increasing porosity.

Although the mathematical solutions in this study can be applied to wastewater treatment system in dye factory for removal of toxic dye molecules by photocatalytic decomposition, it is useful to use a CSTR reactor rather than batch mode reactor. In this study, the bulk concentration in CSTR reactor containing slab-type photocatalytic particles was predicted by solving coupled differential equation using inverse Laplace transform. According to the calculated formula of steady-state concentration of reactant, it could be concluded that the increase of space time in CSTR reactor resulted in the removal of reactant effectively.

ACKNOWLEDGEMENTS

This research was supported by the Industrial Core Technology Development Program (10077545, Development of icephobic coating materials for extreme environment) funded by the Ministry of Trade, industry & Energy (MI, Korea), Priority Research Centers Program through the National Research Foundation of Korea (NRF) funded by the Ministry of Education (NRF-2017R1A6A1 A03015562), and Information & communications Technology Promotion (IITP) grant funded by the Korea Government (MSIT) and Korea Institute for Advancement of Technology (KIAT) grant funded by the Korea Government (MOITIE).

SUPPORTING INFORMATION

Additional information as noted in the text. This information is

available via the Internet at http://www.springer.com/chemistry/journal/11814.

REFERENCES

1. C.-M. Tang and X.-L. Li, *Korean J. Chem. Eng.*, **30**(5), 1119 (2013).
2. T. Murase, E. Iritani, J. H. Cho, S. Nakanomori and M. Shirato, *J. Chem. Eng. Jpn.*, **20**(3), 246 (1987).
3. L. Cao, Q. Fu, Y. Si, B. Ding and J. Yu, *Compos. Commun.*, **10**, 25 (2018).
4. P. Ruckdeschel, A. Philipp and M. Retsch, *Adv. Func. Mater.*, **27**(38), 1702256 (2017).
5. S. T. Lim, J. H. Kim, C. Y. Lee, S. Koo, D.-W. Jerng, S. Wongwises and H. S. Ahn, *Sci. Rep.*, **9**, 10922 (2019).
6. M. Hong, L. Yu, Y. Wang, J. Zhang, Z. Chen, L. Dong, Q. Zan and R. Li, *Chem. Eng. J.*, **359**(1), 363 (2019).
7. Y. Nie, P. M. Witt, A. Agarwal and L. T. Biegler, *Ind. Eng. Chem. Res.*, **52**(44), 15311 (2013).
8. L. Erdei, N. Arecrachakul and S. Vigneswaran, *Sep. Purif. Technol.*, **62**, 382 (2008).
9. C. Xing, Y. Liu, Y. Zhang, J. Liu, T. Zhang, P. Tang, J. Arbiol, de L. Soler, K. Sivula, N. Guijarro, X. Wang, J. Li, R. Du, Y. Zuo, A. Cabot and J. Llorca, *J. Mater. Chem. A*, **7**, 17053 (2019).
10. D. H. Kim and J. Lee, *Korean J. Chem. Eng.*, **29**(1), 42 (2012).
11. W. Cho and J. Lee, *Korean J. Chem. Eng.*, **30**(3), 580 (2013).
12. M. Garg and P. Manohar, *Kuwait J. Sci.*, **40**, 23 (2013).
13. A. N. F. Versypt, P. D. Arendt, D. W. Pack and R. D. Braatz, *Plos One*, **10**, e0135506 (2015).
14. P. Li, G. Xiu and A. E. Rodrigue, *Can. J. Chem. Eng.*, **97**, 217 (2019).
15. Y.-S. Cho, *Korean Chem. Eng. Res.*, **57**(5), 652 (2019).
16. Y.-S. Cho, C. H. Shin and S. Han, *Nanoscale Res. Lett.*, **11**, 46 (2016).
17. Y.-S. Cho and S. H. Roh, *J. Dispers. Sci. Tech.*, **39**(1), 33 (2018).
18. Y.-S. Cho, I.-A. Oh and N. R. Jung, *J. Dispersion Sci. Technol.*, **37**, 676 (2015).
19. Y.-S. Cho, *Korean J. Met. Mater.*, **55**(4), 150 (2017).
20. H. S. Fogler, *Elements of chemical reaction engineering*, 5th Ed., Pearson Education, Inc. New York (2016).
21. T. Pan and B. Zhu, *Chem. Eng. Sci.*, **53**(5), 933 (1998)
22. S. S. S. Cardoso and A. E. Rodrigues, *AIChE J.*, **52**(11), 3924 (2006).
23. N. Milozic, M. Lubej, U. Novak, P. Znidarsic-Plazl and I. Plazl, *Chem. Biochem. Eng. Q.*, **28**(2), 125 (2014).
24. G. Munjal, G. Dwivedi and N. Bhaskarwar, *Int. Proc. Chem. Biol. Environ. Eng.*, **90**, 82 (2015).
25. W. Li, R. Liang, A. Hu, Z. Huang and Y. Norman Zhou, *RSC Adv.*, **4**, 36959 (2014).
26. R. G. Rice and D. D. Do, *Applied mathematics and modeling for chemical engineers*, 1st Ed., John Wiley & Sons, Inc. New York (1995).
27. K. Saito and H. Muso, *Agree to partial differential equation*, 1st Ed., Kodansha, Tokyo (2005).
28. L. K. Campbell, B. K. Na and E. I. Ko, *Chem. Mater.*, **4**(6), 1329 (1992).

Supporting Information

Effect of Biot number on unsteady reaction-diffusion phenomena and analytical solutions of coupled governing equations in porous particles with various shapes

Young-Sang Cho† and Sohyeon Sung

Department of Chemical Engineering and Biotechnology, Korea Polytechnic University,
237 Sangdaehak-ro, Siheung-si, Gyeonggi-do 15073, Korea
(*Received 20 February 2020 • Revised 3 June 2020 • Accepted 7 July 2020*)

Derivation of Concentration inside Cylindrical Particles Subject to Exponentially Decaying Boundary Condition at Particle Surface

After applying the same initial and boundary conditions of spherical particles to unsteady reaction-diffusion equation in cylindrical coordinate, Laplace transform method can be applied to get transient solution, since it may not be complicated compared to eigenfunction expansion method. Since the catalytic particles are initially empty, y(x, 0) vanishes from the following transform result.

$$s\hat{Y}(x, s) - y(x, 0) = \frac{1}{x}\frac{d}{dx}\left(x\frac{d\hat{Y}}{dx}\right) - \phi^2\hat{Y}(x, s) \tag{1}$$

Boundary condition at particle center and surface can be also transformed to yield the following conditions in Laplace domain.

$$\left(\frac{d\hat{Y}}{dx}\right)_{x=0} = 0 \text{ and } \left(\frac{d\hat{Y}}{dx}\right)_{x=1} + Bi\,\widehat{Y}(1, s) = Bi\,\widehat{Y}_b(s) \tag{2}$$

Here, $\widehat{Y}_b(s)$ is the Laplace transform of time-dependent bulk concentration, $y_b(\tau)$. Ordinary differential Eq. (1) in Laplace domain subject to boundary conditions (2) can be solved to yield the following solution.

$$\hat{Y}(x, s) = \frac{BiI_0(\sqrt{(\phi+s)}x)}{\sqrt{\phi^2+s}I_1(\sqrt{\phi^2+s}) + BiI_0(\sqrt{\phi^2+s})}\frac{1}{s+a} \tag{3}$$

By applying residue theorem, the following transient solution in cylindrical coordinate can be obtained from inverse transform of the above equation [1].

$$\begin{aligned} y(x, \tau) = {} & \exp(-a\tau)\frac{I_0(\sqrt{(\phi^2-a)}x)}{I_0(\sqrt{\phi^2-a}) + \frac{\sqrt{\phi^2-a}}{Bi}I_1(\sqrt{\phi^2-a})} \\ & - 2\sum_{n=1}^{\infty}\frac{\lambda_n J_0(\lambda_n x)}{(\lambda_n^2+\phi^2-a)\left[J_1(\lambda_n) + \frac{\lambda_n}{Bi}J_0(\lambda_n)\right]}\exp[-(\lambda_n^2+\phi^2)\tau] \end{aligned} \tag{4}$$

To avoid imaginary number during calculation, the denominator of the first term in the above equation should be $I_0(\sqrt{(a-\phi^2)}) - \frac{\sqrt{a-\phi^2}}{Bi}I_1(\sqrt{a-\phi^2})$, when ϕ^2 is smaller than a. Here, eigenvalue, λ_n satisfies the following transcendental equation.

$$\lambda_n J_1(\lambda_n) = BiJ_0(\lambda_n) \tag{5}$$

REFERENCES

1. R. G. Rice and D. D. Do, *Applied mathematics and modeling for chemical engineers*, 1st Ed., John Wiley & Sons, Inc. New York (1995).